

ISSN 1883 - 0315

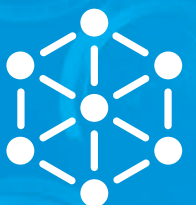


TOHOKU
UNIVERSITY

IMR

KINKEN Research Highlights 2016

Institute for Materials Research, Tohoku University



Research

KINKEN

Research Highlights

2016



Institute for Materials Research, Tohoku University

KINKEN Research Highlights 2016

Contents

Preface	4
----------------------	---

Research Highlights

1. Infrastructural Materials

Microstructure Design of Structural Metallic Materials Division.....	8
Chemical Physics of Non-Crystalline Materials Division	9
Biomaterials Science Division	10
Advanced Crystal Engineering Laboratory	11
Multi-Functional Materials Science Division	12
Deformation Processing Division	13
Analytical Science Division	14
Advanced Materials Development and Integration of Novel Structured Metallic and Inorganic Materials	15
Computational Materials Research Initiative (CMRI)	16

2. Energy-related Materials

Crystal Physics Division	18
Materials Design by Computer Simulation Division.....	19
Irradiation Effects in Nuclear and Their Related Materials Division.....	20
Nuclear Materials Science Division	21
Nuclear Materials Engineering Division.....	22
Non-Equilibrium Materials Division.....	23
Hydrogen Functional Materials Division	24

3. Electronic Materials

Theory of Solid State Physics Division	26
Magnetism Division	27
Surface and Interface Research Division	28
Low Temperature Physics Division	29
Low Temperature Condensed State Physics Division	30
Metal Physics with Quantum Beam Spectroscopy Division	31
Physics of Crystal Defects Division	32
Physics of Electronic Materials Division	33
Solid-State Metal-Complex Chemistry Division.....	34
Magnetic Materials Division.....	35
Crystal Chemistry Division	36
Actinide Materials Science Division	37
Materials Science of Non-Stoichiometric Compounds Division	38

Research Centers

International Research Center for Nuclear Materials Science.....	40
Cooperative Research and Development Center for Advanced Materials	42
High Field Laboratory for Superconducting Materials.....	43
Kansai Center for Industrial Materials Research	44
Center for Computational Materials Science.....	45
Collaborative Research Center on Energy Materials.....	46
International Collaboration Center (ICC-IMR).....	47
Center of Neutron Science for Advanced Materials	48
Research and Development Center for Ultra High Efficiency Nano-Crystalline Soft Magnetic Material	49
Laboratory of Low-Temperature Materials Science	50
Laboratory of Alpha-Ray Emitters	51
Analytical Research Core for Advanced Materials.....	52

Author Index	53
---------------------------	----

Keyword Index	54
----------------------------	----



Preface

Dear Colleagues,

We are pleased to present *KINKEN* Research Highlights 2016, which is the annual report that includes a collection of research outputs of the past year from the Institute for Materials Research (IMR), Tohoku University. *KINKEN* is the abbreviation for “Kinzoku Zairyo Kenkyujo,” the Japanese name for IMR, which is well known in the materials science community.

We are happy to say that IMR celebrates its centenary this year. Professor Kotaro Honda established the IMR at the Tohoku Imperial University in 1916 as the 2nd Division of the Provisional Institute of Physical and Chemical Research. At that time the primary research focus was steel. Thereafter, the research domains gradually broadened to include various types of alloys and metals. The name was changed into the Research Institute for Iron, Steel and Other Metals (RIISOM) in 1922. Subsequently, the institute developed into a global center for fundamental and applied research covering all types of materials, including nonmetals. In 1987 the institute was reorganized into a national collaborative research institute affiliated with Tohoku University, and consequently renamed to the present Institute for Materials Research (IMR).

IMR has greatly contributed to the advancement of materials science and engineering. The invention of KS steel in 1916, the strongest permanent magnet at that time, was the first great achievement. In subsequent years, many different types of practically useable materials have successfully been developed, including new KS steel, Sendust alloy, SiC fibers, various intermetallic compounds, and more recently, amorphous alloys. In addition, considerable effort was dedicated to basic research for



Director



materials development, which paved the way for pioneering research in magnetism, superconductivity, optical properties, and microstructure analyses of materials. Recently, IMR has created a wide array of new materials, including high-performance, high-quality, and multifunctional materials such as bulk metallic glasses, nanostructured materials, nanocomposites, ceramics, crystals, oxides, nitrides, hydrides, complexes, organic materials, etc., which are useful for electronic, optical, magnetic, spintronic, biological, energetic, and infrastructural applications.

In the 21st Century, we face worldwide environmental problems such as global warming and the depletion of resources and energy. There is an increasing need to preserve the environment and work towards achieving sustainable societies. IMR upholds these themes with the objective of “contributing to the well being of the human race and the development of civilization through the creation of new materials that are truly useful to society”.

We hope that the KINKEN Research Highlights will enable you to better understand our recent research activities and will aid the promotion of worldwide collaboration with IMR. We ask for your continued support and welcome any suggestions.

Infrastructural Materials

IMR KINKEN Research Highlights 2016



Enhanced Surface Hardening in Nitriding Process by Dynamic Provision of Nucleation Site For Alloy Nitride Precipitation

Higher surface hardness is required for machinery parts to ensure high reliability and longer life. We found that the combined addition of vanadium and aluminum to iron for nitriding treatment resulted in a significant increase in surface hardness because the vanadium–nitrogen atoms form fine clusters in the early stage and aluminum nitride precipitation is enhanced by the nucleation at the cluster.

Machinery parts such as gears and shafts require high toughness, as well as high hardness, for resistance to wear and fatigue. However, in general, those properties cannot be improved simultaneously. Therefore, surface-hardening processes are performed to harden only the surface region, while the inward region remains ductile. Nitriding is one of the most popular surface-hardening treatments for steel, which improves fatigue-, wear- and corrosion-resistant properties. As compared to other surface-hardening processes, nitriding has advantages in terms of small distortion during the process, higher surface hardness, and better softening resistance at elevated temperatures. The process has thus attracted much attention for the surface hardening of high-precision parts. In the nitriding process, steel parts are held at 500–600°C in a nitriding atmosphere so that nitrogen atoms are absorbed from the surface and then diffuse inward. Surface hardening by nitriding is caused mainly by precipitation of fine alloy nitrides or of alloying element (M)–nitrogen (N) clusters near the surface. Therefore, an understanding of alloy nitride precipitation behavior is crucial to controlling surface hardening by nitriding.

In order to clarify alloying effects on the precipitation of alloy nitrides and the resultant surface hardening, we investigated the microstructure and surface hardness of various nitrided Fe–M binary alloys [1]. It was found that nano-sized M–N clusters formed in the nitriding of Fe–V or Fe–Ti alloys, whereas no precipitation of Al nitrides was observed [1]. As a result, the Fe–Al alloy did not show surface hardening as compared to the other alloys, as shown in Fig. 1 (top). Because Al is also a strong nitride-forming element, its precipitation should be facilitated by introducing nucleation sites.

Recently, we investigated the effects of the combined addition of Al and V atoms, and we found that the addition of V to Fe–Al alloys significantly accelerated the precipitation of Al nitrides, resulting

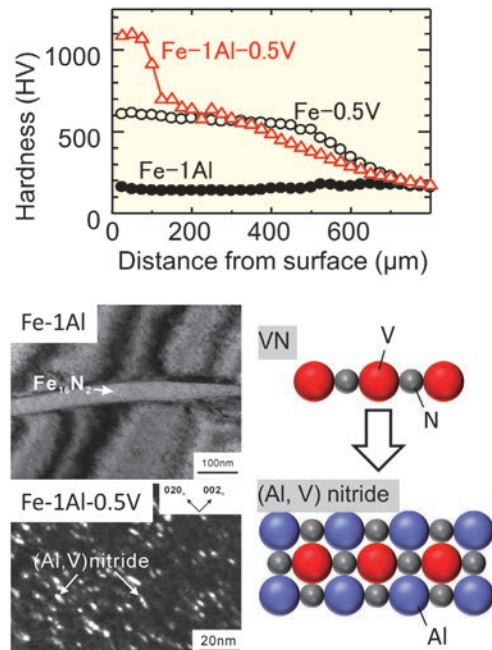


Fig. 1 (top) Hardness–depth profiles of the specimen nitrided at 550°C for 16 h, (bottom left) TEM images of precipitates in Fe–1Al and Fe–1Al–0.5V alloys, and (bottom right) schematic illustration of nucleation of Al nitride at the V–N cluster.

in significant surface hardening [Fig. 1 (top)]. Because the V–N attractive interaction is much stronger than the Al–N one, the formation of V–N clusters take place first, and then precipitation of Al nitrides is induced by nucleation at the V–N cluster/matrix interface at the growth front of the nitrided region [Fig. 1 (bottom)]. Consequently, such dynamic provision of nucleation sites during the nitriding process was found to be very effective for enhanced surface hardening.

References

- [1] G. Miyamoto, Y. Tomio, H. Aota, K. Oh-ishi, K. Hono, and T. Furuhashi, *Mater. Sci. Technol.*, **27**, 742 (2011).
- [2] G. Miyamoto, S. Suetsugu, K. Shinbo, and T. Furuhashi, *Metall. Mater. Trans. A*, **46A**, 5011 (2015).

Keywords: steel, atom probe tomography, nanocluster

Goro Miyamoto (Microstructure Design of Structural Metallic Materials Division)

E-mail: miyamoto@imr.tohoku.ac.jp

URL: <http://www.st-mat.imr.tohoku.ac.jp/en/index.html>

Local Structure around Ge in Lithium– Germanate Glasses

The local structure around Ge in lithium–germanate glasses was investigated by using the anomalous X-ray scattering technique. The averaged coordination number of the first neighboring Ge–O pair increased with increasing Li₂O content up to 24 mol%. The introduction of an octahedral GeO₆ unit is one of the most fundamental structural changes accompanying the so-called germanate anomaly detected in density measurements.

The densities of lithium–germanate glasses show a maximum value at approximately 20 mol% Li₂O [1, 2]. Because the physical properties of glasses correlate with their atomic structures, several advanced analytical studies have been applied for elucidating the structural model for this interesting behavior. We investigated the local structure around Ge in lithium–germanate glasses using anomalous X-ray scattering (AXS) measurements, which is ranked as the most advanced method currently available for obtaining quantitative local structural information for glasses [3].

Lithium–germanate glass samples were prepared by an ordinary melt–quench technique. Powder mixtures of GeO₂ (99.99%) and Li₂CO₃ (99.0%) were calcined at 923 K for 1 h. The prepared samples were melted in a platinum crucible in air for 1 h at 1673 K, and then the melts were quenched by pressing them between two copper plates. The AXS measurements at the Ge *K* absorption edges were performed at the BL-7C beamline of the Photon Factory at the Institute of Material Structure Science, High Energy Accelerator Research Organization.

Figure 1 shows the $\Delta Q_{i\text{Ge}}(Q)$ profiles [4] of four lithium–germanate glasses. Significant differences are observed at the first peak region of approximately 1.8 Å⁻¹, and the peaks decrease and broaden as the Li₂O content increases. Because the first peak is associated with the structure of Ge–Ge pairs, the change detected in the $\Delta Q_{i\text{Ge}}(Q)$ profiles suggests the possible breakdown of the network structure composed of GeO₄ tetrahedra.

The environmental RDFs for Ge calculated by Fourier transformation of the $\Delta Q_{i\text{Ge}}(Q)$ profiles indicated that the distance of the Ge–O pairs increased with increasing Li₂O content. This suggests the introduction of a new local structural unit of GeO₆, as shown in a previous work. Further analysis showed that the fraction of GeO₆ in the lithium–germanate glasses increased with increasing Li₂O content up to 24 mol%. This variation in local structural unit produced a slightly different

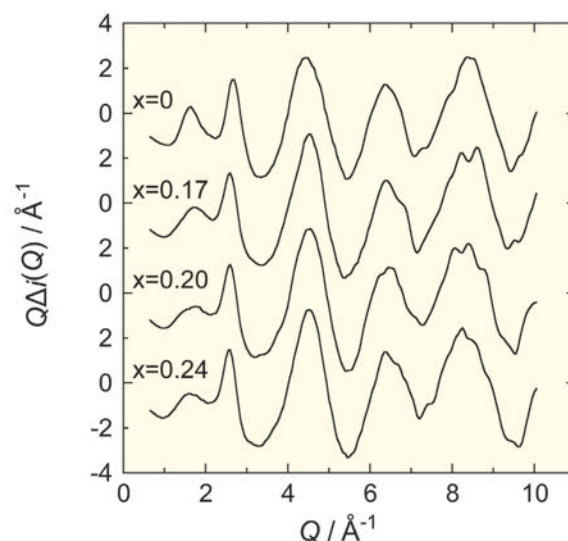


Fig. 1 shows environmental interference functions of $x\text{Li}_2\text{O} - (1-x)\text{GeO}_2$ glasses.

behavior, which was suggested originally by the density measurements. Nevertheless, a similar suggestion was also reported by Henderson and Fleet [5] through a discussion of the observed change in Ge–O distances.

References

- [1] A. O. Ivanov and K. S. Evstropiev, Dokl. Akad. Nauk SSSR **145**, 797 (1962).
- [2] M. K. Murthy and J. Ip, Nature **201**, 285 (1964).
- [3] Y. Waseda, E. Matsubara, and K. Sugiyama, Sci. Rep. RITU **A34**, 1 (1988).
- [4] H. Arima, T. Kawamata, and K. Sugiyama, J. Min. Pet. Sci. **110**, 60 (2015).
- [5] G. S. Henderson and M. E. Fleet, J. Non-Cryst. Solids. **134**, 259 (1991).

Keywords: glass, anomalous X-ray scattering, XAFS

Hiroshi Arima and Kazumasa Sugiyama (Chemical Physics of Non-Crystalline Materials Division)

E-mail: arimah@imr.tohoku.ac.jp

URL: <http://www.xraylab.imr.tohoku.ac.jp/>

Effect of Solid-solute Oxygen Addition on Wear Properties of Biomedical Ti–29Nb–13Ta–4.6Zr Alloy

Ti–29Nb–13Ta–4.6Zr alloy (TNTZ) exhibits good biological and mechanical compatibilities owing to its low toxicity and the fact that its Young’s modulus is close to that of human bone (approximately 60 GPa). Although the wear resistance of titanium alloys is generally poor as a biomaterial, the mechanical strength of TNTZ can be improved by adding an interstitial element, oxygen (O). Thus, the wear characteristics of TNTZ with different oxygen contents were investigated. The volume loss of TNTZ with high O content was significantly lower than that of TNTZ with low O content. Therefore, it is concluded that solid-solution strengthening by oxygen increases the wear resistance of TNTZ.

Wear resistance is one of the most important material properties for biomedical devices with metal-to-metal contact parts because failure can easily occur at such contact parts.

The wear behaviors and mechanisms of two types of titanium alloys were previously analyzed and compared both in air [1] and in Ringer’s solution [2]. The first alloy was a conventional ($\alpha + \beta$)-type Ti–6Al–4V extra-low-interstitial (Ti64) alloy; the second was a newly developed β -type Ti alloy for biomedical applications, Ti–29Nb–13Ta–4.6Zr (TNTZ). It was concluded that volume losses (V_{loss}) of the TNTZ discs and balls were larger than those of the respective Ti64 discs and balls, both in air and in Ringer’s solution. Particularly, when the TNTZ disc slid against the TNTZ ball, V_{loss} of both the disc and ball exhibited maximum values both in air and in Ringer’s solution. These results are related to the severe subsurface deformation of TNTZ, which is caused by the lower resistance of TNTZ to plastic shearing than Ti64, inducing delamination and resulting in a higher wear rate.

Therefore, it is necessary to increase the wear resistance of TNTZ while keeping its Young’s modulus similar to that of human bone. Young’s modulus is related to the crystal structure, which remains essentially unchanged with increasing interstitial element content. Thus, interstitial elements are very promising because their addition to TNTZ is expected to improve its plastic shear resistance via solution strengthening. The wear behavior of TNTZ with oxygen contents of 0.06 and 0.89 mass% (06O and 89O, respectively) were investigated in this study.

The Vickers hardness values of discs and balls made of Ti64, 06O, and 89O were measured. The hardness of the 89O discs was higher than that of the Ti64 discs. Moreover, the hardness of the 89O balls was higher than that of the Ti64 balls. In the case of the 06O material, the hardness of both discs

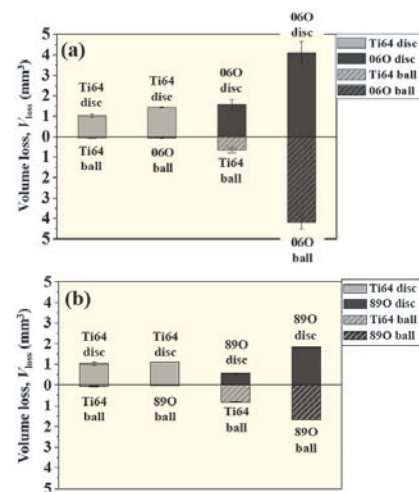


Fig. 1 Volume losses of (a) Ti64/06O combinations and (b) Ti64/89O combinations during frictional wear tests in Ringer’s solution.

and balls was lower than that of the respective Ti64 and 89O discs and balls.

The V_{loss} values of discs and balls made of Ti64, 06O, and 89O subjected to frictional wear tests in Ringer’s solution are shown in Fig. 1. The V_{loss} values of the 89O discs and balls are much lower than those of the 06O discs and balls, regardless of the mating materials. The increase in hardness improved the plastic shear resistance of the 06O discs and balls, which is necessary to avoid severe delamination wear. Therefore, it can be concluded that solid-solution strengthening is a very effective treatment for improving the wear resistance of TNTZ biomedical implants.

References

- [1] Y.-S. Lee, M. Niinomi, M. Nakai, K. Narita, and K. Cho, *J. Mech. Behav. Biomed. Mater.* **41**, 208 (2015).
- [2] Y.-S. Lee, M. Niinomi, M. Nakai, K. Narita, and K. Cho, *Mater. Trans.* **56**, 317 (2015).

Keywords: alloy, biological, mechanical properties
 Mitsuo Niinomi (Biomaterials Science Division)
 E-mail: niinomi@imr.tohoku.ac.jp
 URL: <http://biomat.imr.tohoku.ac.jp/>

Development of Eu:SrI₂ Scintillator Single Crystal and Gamma-ray Detection Devices Using the Eu:SrI₂ Bulk Single Crystal

High-light-yield and high-energy-resolution Eu:SrI₂ gamma-ray scintillator single crystals were developed using a modified micro-pulling-down (μ -PD) method. In addition, Eu:SrI₂ bulk single crystals with diameters of 1–2 in. were grown by a modified Bridgman method using a modified μ -PD furnace. Gamma-ray detection devices using the Eu:SrI₂ bulk single crystal, such as a spectrometer were also developed.

Halide (chloride, bromide, and iodide) materials were investigated owing to their significant potential as scintillator materials with high light yield and high energy resolution. Halide materials have relatively small band-gaps as compared to oxides and fluorides, and the high light yield of halide materials is attributable to this small band-gap. In addition, the high light yield provides high-energy resolution. However, most halide materials have strong hygroscopicity, and it is difficult to grow high-quality and high-transparency single crystals.

Therefore, we developed a modified micro-pulling-down (μ -PD) method for the crystal growth of halide materials [Fig. 1(a)] [1]. In the modified μ -PD method, a removable chamber that can be entered through a glove box filled with high-purity Ar gas is used, thus protecting the inside of the chamber from exposure to outside atmosphere. Therefore, the modified μ -PD method can be used to grow single crystals of halide materials without being affected by outside atmosphere.

Using the modified μ -PD method, we grew Eu:SrI₂ single crystals with high transparency. The light yield and energy resolution were also much higher than those of previous scintillator materials [2].

In addition, we developed a modified Bridgman method using the modified μ -PD furnace for the growth of bulk single crystals because the modified μ -PD method can grow only fiber single crystals. By the modified Bridgman method, we obtained 1 in. Eu:SrI₂ bulk single crystals with various Eu concentrations [3]. By further optimization of the growth conditions, we grew 1.5 and 2 in. Eu:SrI₂ bulk single crystals through collaboration with C&A Corporation [4]. We then developed radiation devices using the bulk Eu:SrI₂ single crystal by the JST project.

Especially, a handheld high-performance spectrometer using the Eu:SrI₂ bulk single crystal was developed in collaboration with Chiyoda Technology Corporation [Fig. 1(b)].

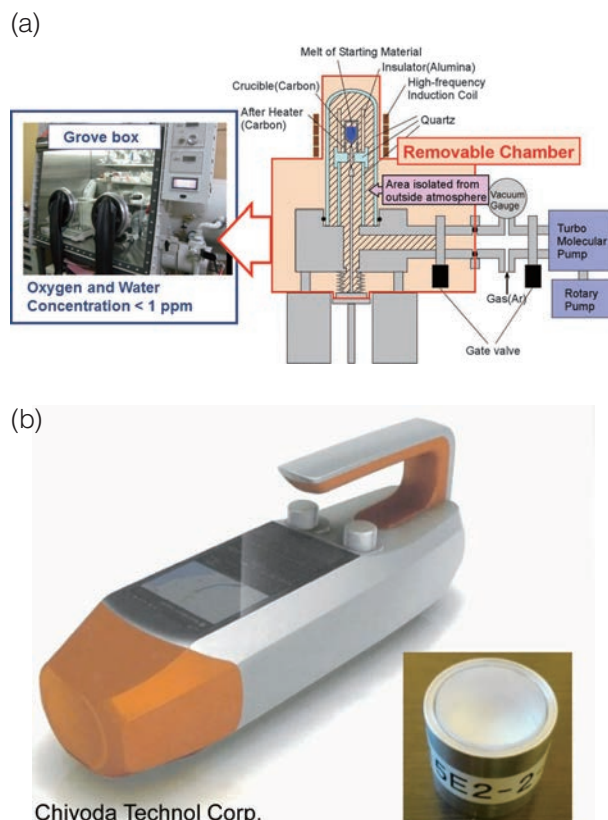


Fig. 1 (a) Schematic of the modified μ -PD method. (b) Spectrometer using Eu:SrI₂ bulk single crystal.

References

- [1] Y. Yokota, N. Kawaguchi, K. Fukuda, T. Yanagida, A. Yoshikawa, and M. Nikl, *J. Cryst. Growth* **318**, 908 (2011).
- [2] Y. Yokota, K. Nishimoto, S. Kurosawa, D. Totsuka, and A. Yoshikawa, *J. Cryst. Growth* **375**, 49 (2013).
- [3] Y. Yokota, S. Kurosawa, K. Nishimoto, K. Kamada, and A. Yoshikawa, *J. Cryst. Growth* **401**, 343 (2014).
- [4] Y. Yokota, T. Ito, S. Yasuhiro, S. Kurosawa, Y. Ohashi, K. Kamada, and A. Yoshikawa, *IEEE Trans. Nucl. Sci.* (2016) accepted.

Keywords: crystal growth, devices, radiation effects

Akira Yoshikawa (Advanced Crystal Engineering Laboratory)

E-mail: yoshikawa@imr.tohoku.ac.jp

URL: <http://yoshikawa-lab.imr.tohoku.ac.jp/index-e.html>

Fine-Structured High-Temperature Non-Oxide Ceramics by Phase Decomposition via Spark Plasma Sintering and Heat Treatment

Transition-metal non-oxide ceramics are promising as ultra-high-temperature ceramics and high-hardness cutting tools. We synthesized dense compacts from Ti- and Zr-based carbide powders by spark plasma sintering, and nano-submicron-sized fine structures were assembled by the subsequent heat treatment. The formation of the self-assembled microstructures enhanced the hardness and toughness.

Ti- and Zr-based non-oxide materials such as TiC, ZrC, TiN, and ZrN have been receiving much attention for use in extremely severe environments, e.g., ultra-high temperature ceramics and cutting tools, because of their high melting point, excellent corrosion resistance, and high hardness. However, for practical use in industry, low sinterability and fracture toughness should be improved. It is difficult to consolidate Ti- and Zr-based non-oxide powders into dense compacts using conventional sintering techniques. In general, a small amount of metals such as Ni and Co is added to promote sintering; however, the metal additives degrade the mechanical properties and corrosion resistance of Ti and Zr carbides. As the powder manufacturing of non-oxide ceramics has developed, it has been of great interest to consolidate pure non-oxide powders and to design dense and high-strength bulk materials by controlling the micro- and nanostructures.

Spark plasma sintering (SPS) is a novel technique to quickly consolidate non-oxide ceramic powders at high temperatures. We consolidated TiC–ZrC composites from TiC and ZrC powders by SPS at sintering temperatures up to 2473 K. At high temperatures above 2273 K, (Ti, Zr)C solid solutions were formed with a fully dense and uniform morphology. Because these dense sintered bodies are pure non-oxide Ti–Zr carbides with no metal sintering additives, the Vickers hardness reached 26 GPa [1, 2]. The sintered bodies of the (Ti, Zr)C solid solutions decomposed into Zr-rich and Ti-rich phases by the subsequent heat treatment at temperatures lower than the sintering temperature (1573–2273 K) [3]. The phase decomposition resulted in the formation of fine nodular structures several tens to hundreds of nanometers in length, with the coherent crystal orientation relationship of the TiC-rich phase {100}//ZrC-rich phase {100}, as shown in Figs. 1(a) and (b). By detailing the effects of TiC–ZrC compositions and heat-treating conditions on the decomposition behavior, we discovered a variety of

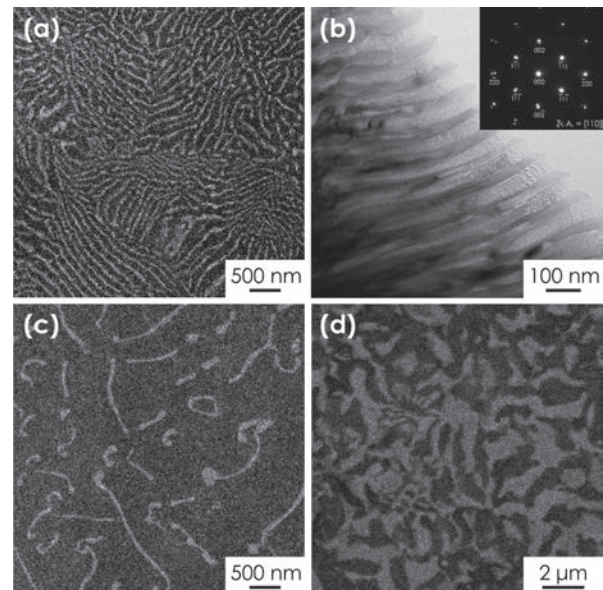


Fig. 1 Phase-decomposed microstructures of TiC–ZrC composites prepared by SPS and the subsequent heat treatment. (a): Fine nodular structure composed of Ti-rich (bright contrast) and Zr-rich (dark contrast) solid solutions. (b): TEM bright-field image and electron diffraction pattern of the several tens of nanometers nodular structure. (c) and (d): Nodular structure and labyrinth structure.

microstructures formed by self-assembling via eutectoid reactions and spinodal decomposition, as shown in Figs. 1(c) and (d). The formation of the fine microstructure enhanced the hardness and fracture toughness [4].

References

- [1] Y. Li, H. Katsui, and T. Goto, *Key. Eng. Mater.* **616**, 52 (2014).
- [2] Y. Li, H. Katsui, and T. Goto, *Ceram. Int.* **41**, 7103 (2015).
- [3] Y. Li, H. Katsui, and T. Goto, *Ceram. Int.* **41**, 14258 (2015).
- [4] Y. Li, H. Katsui, and T. Goto, *J. Eur. Ceram. Soc.* (2016) in press.

Keywords: ceramic, nanostructure, mechanical properties

Takashi Goto, Hirokazu Katsui and Akihiko Ito (Multi-Functional Materials Science Division)

E-mail: goto@imr.tohoku.ac.jp

URL: <http://www.goto.imr.tohoku.ac.jp/>

Regulating the Coarsening of γ' Phase in Superalloys

Stabilizing the γ' phase represents one of the key challenges in developing next-generation superalloys. We fabricated a cobalt-based superalloy with a nanoscale coherent γ' phase, $(\text{Ni},\text{Co})_3(\text{Al},\text{Ti},\text{Nb})$, isolated by stacking-fault ribbons in the alloy matrix as a result of Suzuki segregation of the alloying atoms. This new nanostructure can reduce the coarsening rate of the γ' phase at high temperatures.

One key to preserving the large density of the nanoscale γ' phase while inhibiting its coarsening at high temperatures is to single out an ideal microstructure that can effectively reduce the diffusion among γ' -phase particles without sacrificing the strength of the superalloy. The formation of planar stacking-fault ribbons in superalloys as a result of Suzuki segregation of the alloying elements may fulfill this role.

Here, we developed a new cobalt-based superalloy comprising 35% Ni, 17.5% Cr, 8% Mo, 3% Nb, 2% Al, and 0.8% Ti (mass%) [1]. After cold swaging, the alloy was subjected to aging at 1073 K for 3 h. The nanoscale γ' -phase particles precipitated in the γ matrix [Fig. 1 (a)], whereas the stacking-fault ribbons were formed because of Suzuki segregation of the alloying elements (e.g. Mo and Cr) into these planar defects [2, 3] [Fig. 1 (b)]. The enriched solute atoms (Suzuki segregation) hampered the diffusion of the major elements of the γ' phase (Ni, Al, etc.) across these planar defects, thereby isolating individual γ' -phase nanoparticles and reducing the coarsening rate of the γ' particles during high-temperature exposure [Figs. 1 (c) and (d)]. Furthermore, Suzuki segregation of alloying elements itself can serve as an important additional factor in strengthening superalloys at elevated temperatures (e.g. 973 K).

The developed cobalt-based superalloy demonstrated an extremely high strength of 1250 MPa at 973 K, as indicated in Fig. 2. As compared to commercial superalloys (e.g. Waspaloy®), the developed alloy showed higher yield stress both at room temperature and at elevated temperatures (Fig. 2). Therefore, the present strategy opens a new avenue in producing superalloys with extremely high structural stability at high temperatures and exceptional mechanical properties. In addition, the present alloy showed excellent cold workability. Thus, the application of this method in various structural applications, including heat-resistant springs, is expected.

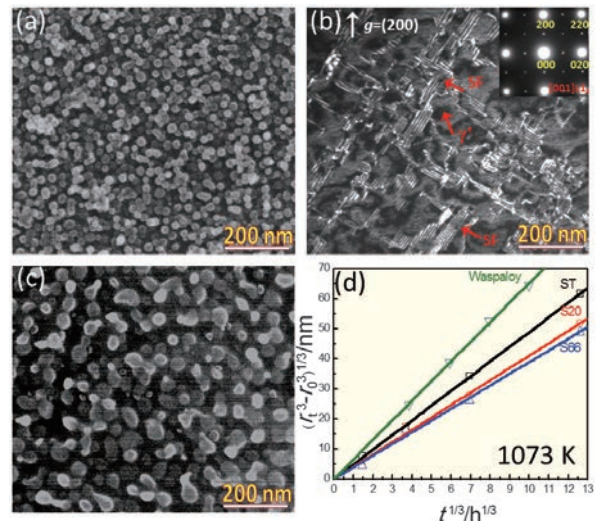


Fig. 1 (a) The morphology of γ' phase in cold-swaged alloy after aging, (b) stacking-fault ribbons, (c) the morphology of γ' phase after aging for 2000 h, and (d) the LSW relationship of the coarsening γ' phase [1].

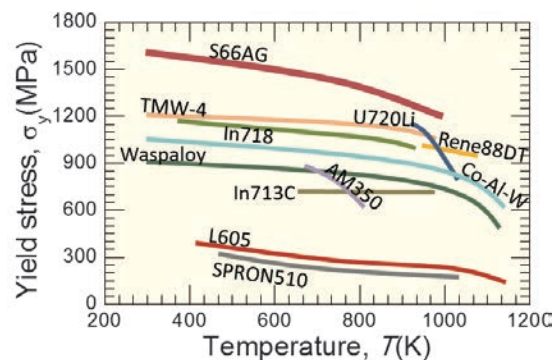


Fig. 2 The temperature dependence of yield stress of the present alloy (S66AG) [1]. The results are compared to those of commercial superalloys such as TMW-4, In718, Waspaloy®, and so on.

References

- [1] H. Bian, X. Xu, Y. Li, Y. Koizumi, Z. Wang, M. Chen, K. Yamanaka, and A. Chiba, *NPG Asia Mater.* **7**, e212 (2015).
- [2] Y. Koizumi, T. Nukaya, S. Suzuki, S. Kurosu, Y. Li, H. Matsumoto, K. Sato, and A. Chiba, *Acta Mater.* **60**, 2901 (2012).
- [3] A. Chiba and M. S. Kim, *Mater. Trans.* **42**, 2112 (2001).

Keywords: alloy, nanostructure, mechanical properties
Akihiko Chiba (Deformation Processing Division)
E-mail: a.chiba@imr.tohoku.ac.jp
URL: <http://www.chibalab.imr.tohoku.ac.jp/>

Distinguishing Rare-earth Magnets Utilizing Portable Cathodoluminescence Spectrometer

We report a method to distinguish neodymium–iron–boron (NdFeB) and samarium–cobalt (Sm–Co) magnets using a portable cathodoluminescence (CL) spectrometer that we realized. Luminescence owing to the NdFeB and Sm–Co magnets was detected by capturing CL images of vacuum-dried residues of respective solutions containing the dissolved NdFeB and Sm–Co magnets. Their luminescent colors were different. Thus, it is possible to distinguish between NdFeB and Sm–Co magnets by obtaining their CL images.

Neodymium–iron–boron (NdFeB) magnets have been used in various products such as electric vehicles and hard disk drives. Among rare-earth elements contained in NdFeB magnets, neodymium, dysprosium, and terbium are expected to be in short supply because of increasing demand. Thus, in the near future, it is expected that these rare-earth elements will need to be recovered from the existing stock of various kinds of magnets. Separation of NdFeB magnets from other magnets such as samarium–cobalt (Sm–Co) magnets is the first step in the recovery process. In the present study, we report a method to distinguish between NdFeB and Sm–Co magnets using a portable cathodoluminescence (CL) spectrometer that we previously realized [1-3]. The portable CL spectrometer detects luminescence emitted from insulating materials or semiconductors by the bombardment of electrons.

Figure 1 (a) shows a schematic of the portable CL spectrometer. The sample was bombarded with focused electrons by changing the temperature of a pyroelectric crystal of LiTaO₃ on which a gold wire was placed at 1 Pa. The luminescence of the sample was detected through a glass viewport using a commercially available camera whose built-in infrared filter was removed. The NdFeB and Sm–Co magnets were each dissolved in hydrochloric acid. Then, the iron in the solutions was removed using methyl isobutyl ketone, and the resulting solutions were dried in vacuum. The dried residues were used as samples.

Figures 1 (b) and (c) show CL images of the dried residues of the Sm–Co and NdFeB magnets, respectively, obtained with the portable CL spectrometer. The dried residue of the Sm–Co magnet produced orange luminescence. This color originated from the luminescent color of the samarium chloride, which has strong peaks at 597 and 647 nm. The dried residue of the NdFeB

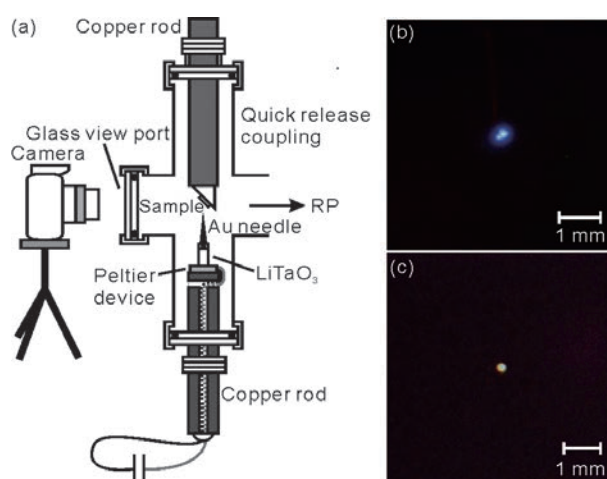


Fig. 1 (a) Schematic of a portable CL spectrometer. CL images of vacuum-dried residues of (b) Sm–Co magnet and (c) NdFeB magnet.

produced blue.

This luminescence was detected through a filter cut light with wavelengths less than 780 nm. Thus, this color was ascribed from the infrared luminescence of neodymium chloride, whose strongest peaks occur at 878 and 892 nm. The portable CL spectrometer can therefore distinguish between NdFeB magnets and Sm–Co magnets by the luminescent colors of their CL images.

References

- [1] S. Imashuku and J. Kawai, *Microsc. Microanal.* **21**(S3), 793 (2015).
- [2] S. Imashuku, I. Ohtani, and J. Kawai, *Proceedings of ALC '15*, 27p-P-48 (2015).
- [3] S. Imashuku, K. Wagatsuma, and J. Kawai, *Microsc. Microanal.* **22**, 82 (2016).

Keywords: electron irradiation, spectroscopy, cathodoluminescence
 Susumu Imashuku (Analytical Science Division)
 E-mail: susumu.imashuku@imr.tohoku.ac.jp
 URL: <http://wagatsuma.imr.tohoku.ac.jp/>

Biocompatibility of Ni- and Be-free Ti-based Bulk Metallic Glasses

Ti-based (Ti–Zr–Cu–Pd–Sn) bulk metallic glasses (BMGs) exhibited significant glass-forming ability, high strength, high thermal stability, low stress corrosion cracking susceptibility, and good bioactivity. *In vivo* implant evaluation showed that it had good tissue compatibility, equivalent bone integration, and the ability to bond with the Ti sample. It is thus possible to use Ti-based BMGs in biomedical applications.

Ti-based bulk metallic glasses (BMGs) are promising materials for applications in biomedical fields owing to their high corrosion resistance, excellent mechanical properties, and good biocompatibility. Many Ti-based BMGs have been developed in the framework of Ti–Ni–Cu and Ti–Zr–Cu–Ni alloy systems. However, these Ti-based BMGs contain Ni, Be, etc., which are unsuitable for use in the human body because of their cellular toxicity, limiting the application of Ti-based BMGs in biomedical fields. We developed Ni- and Be-free Ti–Zr–Cu–Pd BMGs with high strength and good corrosion resistance, showing that it is possible to create novel Ti-based BMG implants [1]. However, the relatively low glass-forming ability (GFA) (with a critical diameter of 7 mm) of these BMGs restricts their use in biomedical applications. Large critical diameters and excellent mechanical properties are fundamental requirements for such BMGs.

We investigated the influence of small amounts of additional elements on the formation and properties of Ti–Zr–Cu–Pd bulk glassy alloys. Minor Sn addition improved the glass-forming ability, thermal stability, and plasticity of the Ti–Zr–Cu–Pd alloy system [2]. The stress corrosion cracking (SCC) behavior in Hanks' solution and the bioactivity of Ti–Zr–Cu–Pd–Sn BMGs were also investigated. The results revealed that the Ti-based BMGs exhibited low SCC susceptibility in simulated body fluid. A bioactive calcium phosphate compound layer was obtained after two-step treatment on the Ti-based BMGs [3].

We implanted bars of the developed Ti–Zr–Cu–Pd–Sn BMG in the femoral bones of rats, followed by investigation of the local tissue reaction, as well as of local and whole-body component ion diffusion. After 12 weeks' implantation, inflammatory reactions, implant dislocation, or loosening were not observed in any of the cases. *In vivo* implant evaluation showed that the Ti-based BMG had good tissue compatibility, equivalent bone integration, and the ability to bond with the Ti sample (Fig. 1). No component ion diffusion was detected up to 3 months' post implantation (Fig. 2) [4]. Thus, the

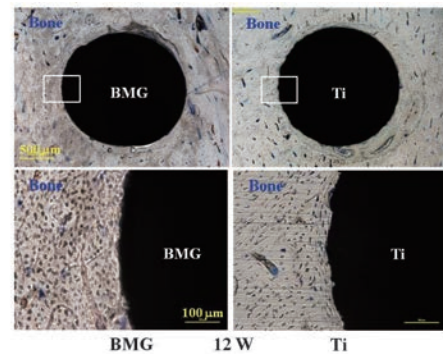


Fig. 1 Histological views of Ti-based BMG implant and Ti implant [4]. Both samples are well covered by surrounding bone tissue. There were no abnormal findings in the surrounding bone tissue. Objective magnification of the upper images is $\times 4$ and that of the lower images is $\times 20$.

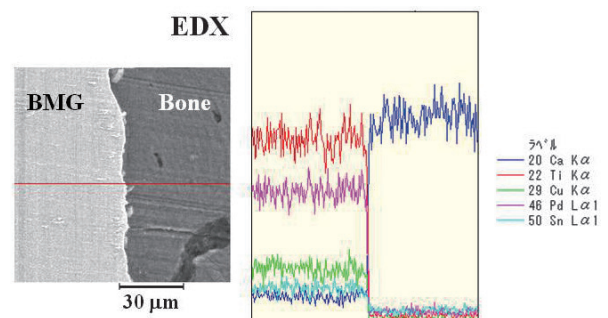


Fig. 2 EDX elemental analysis of implant border area [4]. No diffusion of any metallic ions in the BMG sample was found.

feasibility and efficacy of Ti-based BMGs for use as bone implants was confirmed.

References

- [1] S. L. Zhu, X. M. Wang, F. X. Qin, M. Yoshimura, and A. Inoue, *Mater. Trans.* **48**, 2445 (2007).
- [2] S. L. Zhu, G. Q. Xie, A. Inoue, Z.D. Cui, X. J. Yang, and W. Zhang, *Mater. Sci. Forum* **833**, 79 (2015).
- [3] F. X. Qin, S.L. Zhu, Z. H. Dan, A. Kawashima, and G. Q. Xie, *J. Alloys Compd.* **615**, S123 (2014).
- [4] R. Kokubun, W. Wang, S. L. Zhu, G. Q. Xie, S. Ichinose, S. Itoh, and K. Takakuda, *Bio-Med. Mater. Eng.* **26**, 9 (2015).

Keywords: bulk metallic glass, biological, mechanical properties

Guoqiang Xie (Advanced Materials Development and Integration of Novel Structured Metallic and Inorganic Materials)

E-mail: xieqg@imr.tohoku.ac.jp

URL: <http://amdi-pro.imr.tohoku.ac.jp/en/index.html>

Positron–Monovacancy Interaction in d-Block Metals

Dr. Ishibashi is a core member of CMRI and has been conducting numerous studies based on positrons, which are known as powerful probes for detecting vacancy-type defects in various solids. Combined with theoretical calculations, it has become possible to identify defect species. The effect of a trapped positron on the monovacancy structure was systematically investigated. The present results are useful in predicting positron annihilation parameters accurately.

To describe the positron state in solids, Boroński and Nieminen proposed the two-component density-functional-theory formalism [1], with which interactions between a positron and electrons, as well as between a positron and nuclei, are explicitly described. In many practical calculations, a simplification is made assuming that the positron affects neither the electronic structure nor the atomic arrangement. This simplified scheme is called the “conventional scheme”. The presence of a trapped positron affects the electronic structure and the atomic arrangement at a certain level, depending on the material being investigated. With both conventional and two-component DFT schemes, we recently calculated Doppler-broadening spectra and positron lifetimes for divacancies in C, Si, Ge, SiC, AlN, GaN, and InN, and we found that the difference between the two schemes depends on the bulk modulus [2]. For relatively soft materials, Si and Ge, the difference is significant. In the present study, we expanded our investigation to the positron–monovacancy interaction in d-block metals (except for Mn, Tc, and Hg) [3].

All the calculations were performed using our computational code QMAS (Quantum MAterials Simulator). In the conventional scheme, electronic structures, if necessary, and atomic positions are calculated independently of the presence of a positron. On the other hand, in the two-component scheme, electronic structures and atomic positions (when they are relaxed) are affected by the presence of a positron. Calculations were performed on supercells with sizes of $4 \times 4 \times 2$ for hcp, $3 \times 3 \times 3$ for fcc, and $4 \times 4 \times 4$ for bcc. Further details are described in Ref. [3].

Figure 1 represents the positron density distribution trapped at a monovacancy in bcc Fe as an example of the obtained results. Differences between the positron lifetimes obtained by the two schemes, $\Delta\tau$, are plotted in Fig. 2 as a function of the atomic number, Z . For the unrelaxed structure, the positron lifetime calculated with the presence of a positron is generally longer than that obtained neglecting the positron

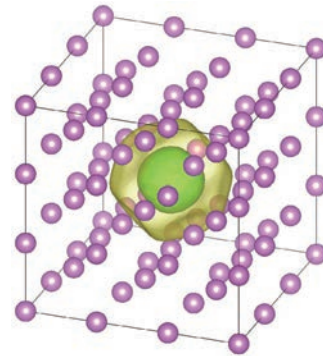


Fig. 1 Positron density distribution trapped at a monovacancy in bcc Fe. Two levels of isosurfaces are shown.

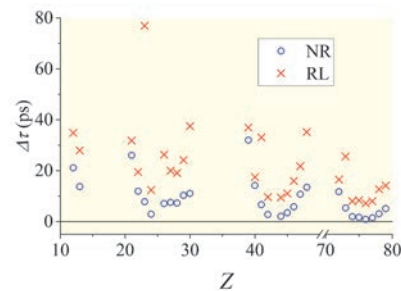


Fig. 2 Z-dependence of the differences in positron lifetimes trapped at a monovacancy, $\Delta\tau$, calculated with no relaxation (NR) and relaxation (RL).

effect. When the atomic positions are relaxed without the positron effect, for most cases, inward relaxation of the atoms surrounding the monovacancy is observed. However, this relaxation is suppressed when the positron effect is taken into account. Thus, the difference in the positron lifetime is widened, especially for the group V metals. As is the case for semiconductors, these differences are also related to the bulk modulus and the cohesive energy [3].

References

- [1] E. Boroński and R. M. Nieminen, *Phys. Rev. B* **34**, 3820 (1986).
- [2] S. Ishibashi and A. Uedono, *J. Phys.: Conf. Ser.* **674**, 012020 (2016).
- [3] S. Ishibashi, *J. Phys. Soc. Jpn.* **84**, 083703 (2015).

Keywords: positron annihilation, first-principles calculations, vacancy

Shoji Ishibashi [Research Center for Computational Design of Advanced Functional Materials (CD-FMat), AIST]

E-mail: shoji.ishibashi@aist.go.jp

Tetsuo Mohri (Project Leader of Computational Materials Research Initiative)

E-mail: tmohri@imr.tohoku.ac.jp

Energy-related Materials

IMR KINKEN Research Highlights 2016 

Development of Crystal Growth Technology for Producing High-quality Multicrystalline Si Ingots for Solar Cells

Growth technology for obtaining a high-quality multicrystalline Si (mc-Si) ingot for solar cells is developed on the basis of the concept that mc-Si ingots grow under non-wetting/non-reacting conditions. The mc-Si ingot grown under such conditions had a higher minority carrier lifetime than the mc-Si ingot grown using a conventional method. This technology will be a powerful tool for realizing high-performance solar cells.

In the photovoltaic market, solar cells made of polycrystalline Si (commonly expressed as multicrystalline Si, mc-Si) are the main products both at present and potentially in the future by totally considering the production cost, storage of raw materials, safety, reliability, and energy conversion efficiency of the solar cells. However, in the conventional method for growing mc-Si ingots, it is difficult to avoid contaminating the mc-Si ingot with impurities during the melting/solidification process, where impurities in the Si_3N_4 powder used to coat the crucible dissolve into the Si melt. Si_3N_4 powder can also detach from the crucible and be dissolved into the Si melt. Such impurities act as a lifetime killer and a source of dislocations, which degrades the quality of the mc-Si ingots.

We had an idea that if a mc-Si ingot could be grown under non-wetting and non-reacting conditions, the problem of impurity contamination during the growth process would be solved. Therefore, the growth conditions, including the crucible material and coating, atmosphere, and thermal history during the melting/growth process were systematically investigated.

Figure 1 shows the top surfaces of as-grown mc-Si ingots grown using our method and a conventional method [1]. The difference in the shininess of both ingot surfaces is evident. Although inclusions of Si_3N_4 powder are observed on the surface of the ingot grown using the conventional method, no such inclusions are observed in the ingot grown using our method, which is thus much shinier. The side and bottom surfaces of both as-grown mc-Si ingots are also shown in Fig. 1. The surfaces of the ingot grown in our method are very smooth and shiny, whereas the grain structures are not visible, while the surfaces of the ingot grown in the conventional method were rough and the grain structures were visible. The minority carrier lifetime of our ingot was much higher than that of the conventionally grown mc-Si ingot. These results

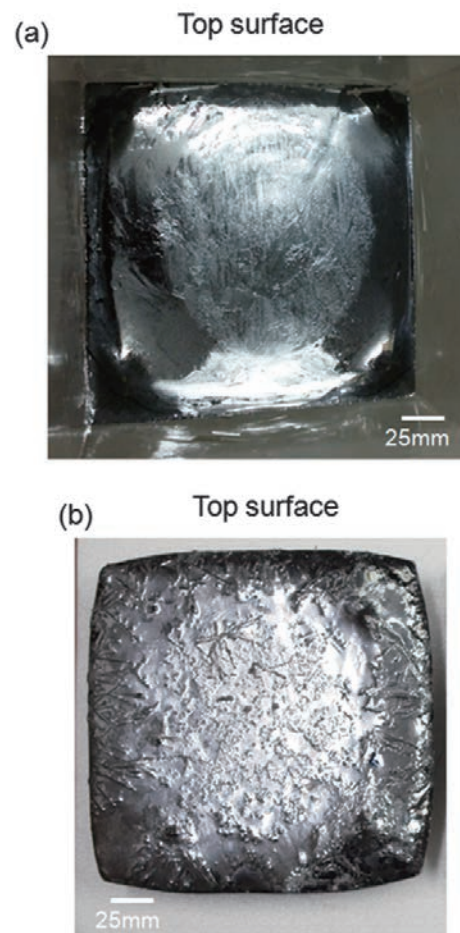


Fig. 1 (a) Top surfaces of as-grown mc-Si ingots grown under (a) a non-wetting and (b) conventional conditions.

indicate that our technology has the potential to be a powerful tool in the near future for the production of high-quality mc-Si ingots for solar cell applications.

References

- [1] K. Fujiwara, Y. Horioka, and S. Sakuragi, *Energy Science & Engineering* **3**, 419-422, (2015).

Keywords: crystal growth, solar cells
 Kozo Fujiwara (Crystal Physics Division)
 E-mail: kozo@imr.tohoku.ac.jp
 URL: <http://www.xtalphys.imr.tohoku.ac.jp/>

Application of Multi-physics Simulator Based on Molecular Dynamics Method for Materials Design

Next-generation materials design strongly requires a deep understanding of multi-physics phenomena, including chemical reactions, impacts, fluid, heat, etc. We applied our developed multi-physics computational simulator based on the molecular dynamics method to the complicated multi-physics phenomena and processes, contributing to the materials design related to the mechanical engineering such as fuel cells, electronics, etc.

Highly functional and high-performance materials are necessary in a wide variety of research fields such as fuel cells, electronics, tribology, etc. in order to solve energy and environmental problems and to realize a safe and secure society. Recently, a deeper understanding of multi-physics phenomena, including chemical reactions, impacts, fluid, heat, etc. is required for designing material and system technologies. However, traditional simulation methods such as first-principles calculations and fluid mechanics cannot simulate such multi-physics phenomena. Therefore, we applied our multi-physics simulator, which was based on tight-binding molecular dynamics, molecular dynamics, etc., to pioneering next-generation materials design [1-2].

In solid oxide fuel cells, which are expected to be next-generation power generators, the anode material, consisting of Ni and ceramic nanoparticles, needs to exhibit durability during sintering of the Ni particles. Therefore, we performed a multi-nanoparticle sintering simulation and investigated the different sintering processes for Ni/YSZ and Ni/ScSZ nanoparticles. The degree of sintering of the Ni nanoparticles in the Ni/YSZ model shown in Fig. 1(a) is larger than that in the Ni/ScSZ model shown in Fig. 1(b). This indicates that Ni/ScSZ provides more durability to sintering. Our multi-nanoparticle sintering simulator is therefore useful for designing durable, high-performance anodes [1].

Hydrogenated amorphous silicon carbide (α -Si_xC_yH_z) is expected to be applicable to electronic and optical devices. The atomic fractions in the plasma-enhanced chemical vapor deposition (CVD) process are important in terms of the performance of the carbide. Thus, we performed a CVD growth simulation of α -Si_xC_yH_z, where CH₃ or SiH₃ radicals are irradiated to a Si substrate (Fig. 2). In the simulation, a surface-adsorbed CH₂ species with a dangling bond (DB) is generated and then inserted into a neighboring Si–Si bond, converting it to a Si–C bond. The bond rearrangement transfers the DB from the C to the Si atoms. A CH₃ radical is then adsorbed

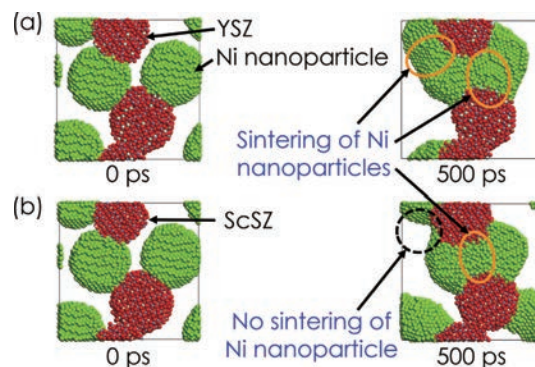


Fig. 1 Cross-sectional snapshots of time evolution of (a) Ni/YSZ and (b) Ni/ScSZ multi-nanoparticle models.

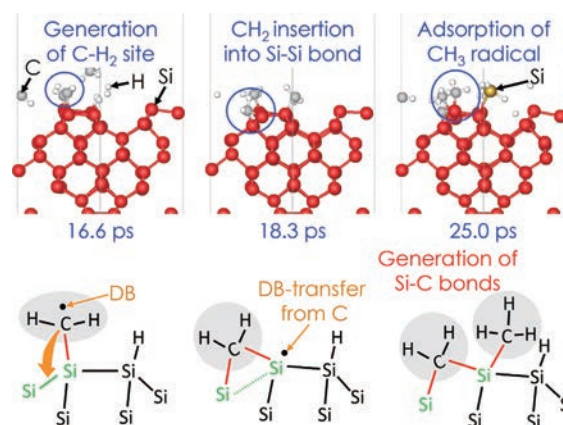


Fig. 2 Snapshots of CVD simulation with the continuous impingement of CH₃ and SiH₃ radicals. (Bottom) Schematic images corresponding to each configuration.

on the Si atom, forming a Si–C bond. The absence of DBs on the C atoms suppresses the formation of C–C bonds. We thus found the reason why Si–C bonds are preferentially formed instead of C–C bonds in the CVD process [2].

References

- [1] J. Xu, S. Bai, Y. Higuchi, N. Ozawa, K. Sato, T. Hashida, and M. Kubo, *J. Mater. Chem. A* **3**, 21518 (2015).
- [2] T. Kuwahara, H. Ito, K. Kawaguchi, Y. Higuchi, N. Ozawa, and M. Kubo, *J. Phys. Chem. C* **120**, 2615 (2016).

The Diffusivity and Solubility of Copper in a Reactor Pressure Vessel Steel Studied by Atom Probe Tomography

The diffusion coefficient, D , and the solubility limit, c , of copper (Cu) in nuclear reactor pressure vessel (RPV) steels are important parameters for understanding the Cu precipitation, which causes irradiation-induced embrittlement of RPV steels. By using atom probe tomography, the values of D and c were directly measured at lower temperatures close to the real conditions for RPV steels in operation.

Copper (Cu) precipitation plays an important role in the irradiation-induced hardening of nuclear reactor pressure vessel (RPV) steels. Thus, the diffusion coefficient, D , and the solubility limit, c , of Cu in RPV steels are important parameters for understanding the kinetics of precipitation.

The D and c values of Cu in iron (Fe) are measured at temperatures higher than ~ 700 °C because conventional techniques require long-range diffusion over distances of at least several micrometers due to the spatial resolution limit. Therefore, the values of D and c at ~ 300 °C, which is the temperature of RPVs used in light-water reactors in operation, are generally determined by extrapolation from the limited temperature range, leading to potential uncertainties. Direct measurements of D and c at lower temperatures are necessary for accurate determination, but they have not yet been obtained.

We recently employed atom probe tomography (APT) to observe the very short-range (several tens of nanometers) diffusion of Cu in an Fe matrix [1]. Diffusion couples of Cu–Fe were annealed and the penetration of Cu into Fe was observed by APT. The D and c values of Cu in Fe were directly measured at temperatures from 550 to 750 °C, temperatures that are 150 °C lower than temperatures used in previous studies. In this study, the same method was applied to study the D and c values of Cu in A533B steel, a typical RPV steel [2]. A533B was electropolished and coated with Cu using vapor deposition, followed by annealing under three conditions: 550 °C for 1,008,000 s, 600 °C for 250,000 s, and 700 °C for 3,000 s.

Figure 1 shows a typical set of atom maps for Cu and Fe obtained for the A533B specimen annealed at 700 °C. The diffusion of Cu into A533B is clearly observed. The D and c values were determined by applying Fick's second law to the concentration profiles of Cu assuming a concentration-independent diffusion coefficient, a semi-infinite medium, and a constant surface concentration.

Figure 2 shows the Arrhenius plot of D as a

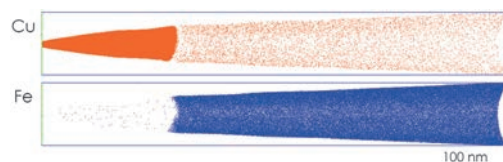


Fig. 1 Atom maps for Cu and Fe for the A533B specimen annealed at 700 °C for 3,000 s.

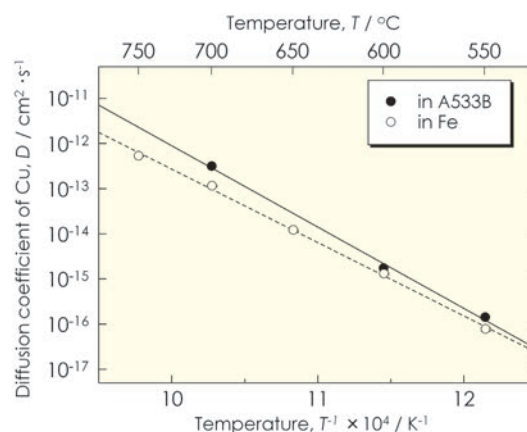


Fig. 2 Arrhenius plot for diffusion coefficient of Cu in A533B steel and that in pure Fe.

function of temperature in A533B steel and in pure Fe. The obtained dataset was well-fitted using the Arrhenius equation, $D = D_0 \exp(-Q/k_B T)$, where D_0 is the pre-exponential factor of $89 \text{ m}^2/\text{s}$ and Q is the activation energy of $3.45 \times 10^5 \text{ J/mol}$. It was found that the activation energy for the A533B steel was higher than that for Fe, $Q = 3.11 \times 10^5 \text{ J/mol}$. It was also revealed that the c value in A533B was almost the same as that in Fe at temperatures ranging from 550 to 700 °C.

References

- [1] T. Toyama, F. Takahama, A. Kuramoto, H. Takamizawa, Y. Nozawa, N. Ebisawa, M. Shimodaira, Y. Shimizu, K. Inoue, and Y. Nagai, *Scripta Mater.* **83**, 5 (2014).
- [2] M. Shimodaira, T. Toyama, F. Takahama, N. Ebisawa, Y. Nozawa, Y. Shimizu, K. Inoue, and Y. Nagai, *Mater. Trans.* **56**, 1513 (2015).

Keywords: atom probe tomography, nuclear materials, diffusion

Yasuyoshi Nagai, Koji Inoue, Yasuo Shimizu, Kazuaki Nagumo (Irradiation Effects in Nuclear and Their Related Materials Division)

E-mail: nagai@imr.tohoku.ac.jp

URL: <http://wani.imr.tohoku.ac.jp/>

Dynamic Observation of Hydrogen Behavior by Particle Scattering Combined with Optical Measurements

We applied ion beam analysis techniques combined with optical analysis to investigate the hydrogen behavior in functional materials under an irradiation environment. Simultaneous measurements of hydrogen and light emission revealed the trapping and release mechanism of hydrogen in connection with the implantation-induced damage in functional materials.

Ion beam analysis (IBA) techniques are powerful and unique tools used to determine the atomic concentration as a function of depth to several microns. The fast and non-destructive characteristics of IBA allow *in-situ* observation of time-dependent phenomena in functional materials [1]. For example, the investigation of compositional changes in a thin film during the anodizing process gives us a better understanding of the formation mechanism of the corrosion-resistant surface [2]. IBA is also useful for examining hydrogen transport behavior in energy production and storage, such as in electrolytes for batteries and fuel cells [3], solid breeders for fusion reactors, and polymer films for radiation measurements [4].

Li-based oxides are regarded as candidates for use as breeder materials for multiplying hydrogen isotopes as the fuel in fusion. Since hydrogen interacts strongly with defects, it is able to know the hydrogen behavior by examining optical characteristics that are sensitive to defects in oxides. The luminescence from LiTaO_3 decreased with increasing incident D ion fluence, as shown in Fig. 1. After stopping the implantation, the subsequent heat treatment showed recovery of the luminescence intensity with increasing release of D atoms from the implanted depth, indicating implantation-induced defect trapping of D atoms. According to the ion channeling along the $\langle 0001 \rangle$ and $\langle 11-20 \rangle$ axes directions, D atoms are considered to be located preferably at the substitutional sites of the Li sublattice in the LiTaO_3 crystal.

Luminescent materials are attractive for making scintillators for radiation detection. Polyethylene naphthalate (PEN), consisting of two benzene rings, exhibits strong blue luminescence in response to irradiation. Generally, the optical properties of organic materials are altered effectively and permanently by ionizing radiation. In the case of the PEN film, air exposure caused the recovery of luminescence, accompanied by the immediate accumulation of H atoms in the ion-implanted region, whereas the O concentration did not change, as shown in Fig. 2.

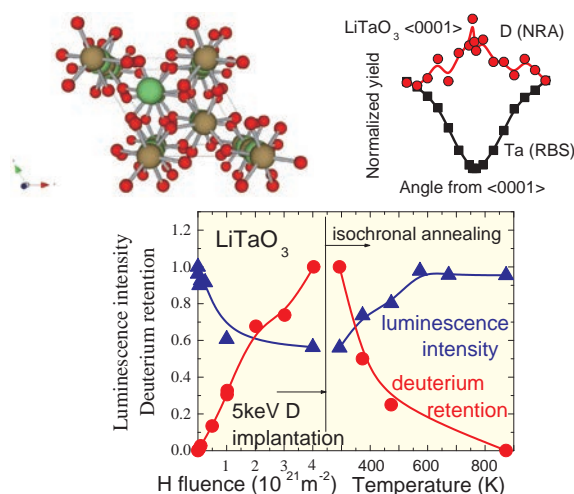


Fig. 1 Luminescence intensity and D retention in the LiTaO_3 crystal during ion implantation and the subsequent heat treatment. The angular scan yields along the $\langle 0001 \rangle$ axis are inserted in the upper part.

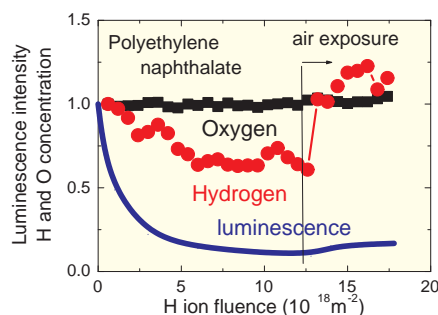


Fig. 2 H and O concentrations and the luminescence intensity in the surface layer of the PEN film during the 1 MeV H implantation and air exposure.

References

- [1] S. Nagata, H. Katsui, K. Hoshi, B. Tsuchiya, K. Toh, M. Zhao, T. Shikama, and E.R. Hodgson, *J. Nucl. Mater.* **442**, 501 (2013).
- [2] K. Shahzad, E. Tsuji, Y. Aoki, S. Nagata, and H. Habazaki, *Electrochim. Acta* **151**, 363 (2015)
- [3] B. Tsuchiya, K. Morita, S. Nagata, T. Kato, Y. Iriyama, H. Tsuchida, and T. Majima, *Surf. Interf. Anal.* **46**, 1187 (2014)
- [4] S. Nagata, M. Mitsuzuka, S. Onodera, T. Yaegashi, K. Hoshi, M. Zhao, and T. Shikama, *Nucl. Instr. Meth. Phys. Res. B* **315**, 157 (2013).

Keywords: ion beam analysis, luminescence, hydrogen implantation

Shinji Nagata (Nuclear Materials Science Division)

E-mail: nagata@imr.tohoku.ac.jp

URL: <http://www-lab.imr.tohoku.ac.jp/~wshikama/>

Modeling of One-dimensional Migration of Self-interstitial Atom Clusters in Steels for Nuclear Materials

We propose a new mechanism for one-dimensional (1D) migration of self-interstitial atom (SIA) clusters in concentrated alloys induced by high-energy particle irradiation. The model explains *in-situ* observation of 1D migration in various steels used for nuclear power plants under electron irradiation using high-voltage electron microscopy.

Recent theoretical and experimental studies have confirmed that small interstitial atom (SIA) clusters in pure metals make a gliding motion along the direction of the Burgers vector with low activation energies, called one-dimensional (1D) migration. This phenomenon has been suggested to affect defect structural development under irradiation with high-energy particles, such as void swelling. Although 1D migration processes in practical alloys have technical and fundamental significance for developing materials for nuclear power applications, they are not well understood.

We propose a mechanism for 1D migration in concentrated alloys driven by high-energy particle irradiation, called “radiation-induced glide motion” [1]. SIA clusters are fundamentally mobile on their respective 1D migration tracks, but in concentrated random alloys they are stationary at the position where the fluctuating formation energy achieves a local minimum. Irradiation successively alters the microscopic distribution of solute atoms from one random distribution to another through atomic displacements and the subsequent recovery of the produced point defects. The interatomic mixing changes the stable cluster position on the track and causes the clusters’ 1D migration into a new stable position. Moreover, growth and shrinkage of interstitial clusters under irradiation changes the microscopic distribution of solute atoms around the loop dislocation itself, which results in another 1D migration.

Molecular dynamics simulations revealed the occurrence of stepwise 1D migration in Fe–Cu alloys under exchanges of atoms or cluster shrinkage: a single 1D migration was induced on average by two exchanges per atom or a cluster radius change by two interatomic distances. The 1D migration distance ranged up to several nanometers. The model explained experimental 1D migration in various alloys under *in-situ* observation using high-voltage electron microscopy [2]. The short-range 1D migration (<10 nm) of SIA clusters reflects the wavelength of the fluctuation of the formation energy

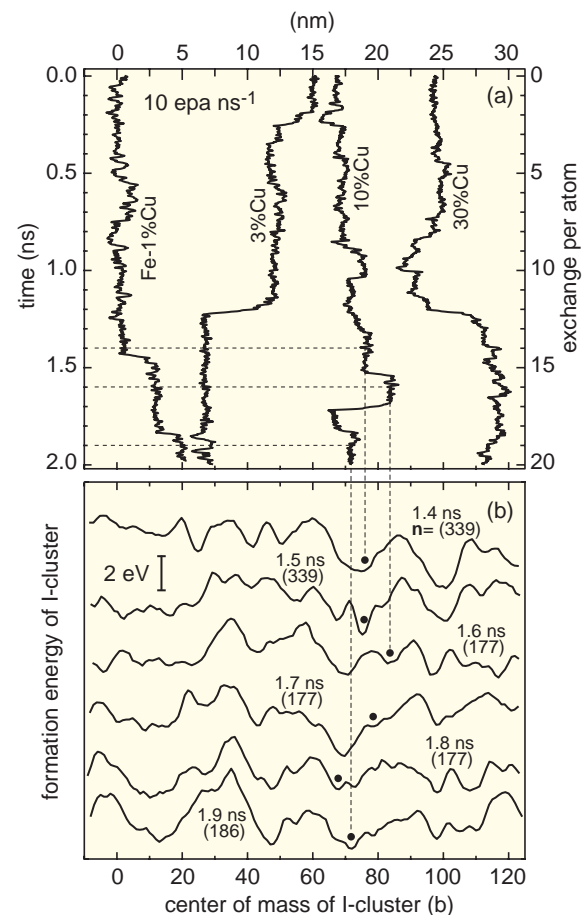


Fig. 1 (a) Results of molecular dynamics simulation on trajectory of center of mass of SIA clusters (217i) under random exchanges of first-nearest pair of atoms in Fe–Cu alloys. (b) Variation of the formation energy profile and the plane of the interstitial cluster in Fe–10%Cu [1].

of SIA clusters, which gives the characteristic length of 1D migration in concentrated alloys.

References

- [1] Y. Satoh, H. Abe, and T. Matsunaga, *Philos. Mag.* **94**, 2170 (2014).
- [2] Y. Satoh, H. Abe, Y. Matsukawa, T. Matsunaga, S. Kano, S. Arai, Y. Yamamoto, and N. Tanaka, *Philos. Mag.* **95**, 1587 (2015).

Keywords: nuclear materials, electron irradiation, simulation
Yuhki Satoh (Nuclear Materials Engineering Division)
E-mail: ysatoh@imr.tohoku.ac.jp

Three-dimensional Bicontinuous Porous Carbon Generated in Low-Temperature Metallic Liquid

A three-dimensional bicontinuous porous carbon (3Dbp-carbon) with a well-developed graphite structure was generated by dealloying in a metallic melt at low temperatures. Both X-ray diffraction and the Raman spectra indicated that 3Dbp-carbon became more ordered after the graphitization process. However, the surface area and total pore volume did not significantly decrease, indicating that porous graphite with extremely high electron conductivity and durability can be obtained by optimizing the dealloying and the subsequent activation processes.

Carbon black (CB) is commonly used for electrode materials because of its several advantages. Nevertheless, CB has problems such as high electrical resistivity and low durability owing to its low crystallinity. Graphitization is one of the most effective methods of increasing the graphite ratio of carbon-based materials, but it also decreases the surface area and pore volume of carbon-based materials such as CB, such that the micropores mostly disappear because of thermal instability. If porous carbon consisting of meso- and macro pores can be generated, the surface area and pore volume originating from these pores should remain after graphitization because of its high thermal stability. To synthesize these new carbon materials, we previously developed a dealloying process in a metallic melt [1, 2], a simple top-down process for fabricating three-dimensional bicontinuous porous carbon.

In the current study, we synthesized 3Dbp-carbon by immersing a precursor of $Mn_{85}C_{15}$ (at%) in a pure Bi melt at 1073 K. Because Mn is miscible with Bi but carbon is not, only Mn atoms dissolved in the Bi melt, and the unstable carbon atoms spontaneously organized into a nanoporous structure.

Fig. 1(a) and 1(b) show SEM images of the products. Two types of porous materials with different porosities were found. When the $Mn_{85}C_{15}$ precursor, consisting of α -Mn and $Mn_{23}C_6$, was dipped into the Bi melt, α -Mn first reacted with the Bi melt to selectively dissolve Mn atoms; the remaining carbon atoms then diffused on the boundary between the precursor and the Bi melt, resulting in self-organized 3Dbp-carbon with a relatively high porosity (Fig. 1(a)). Then, $Mn_{23}C_6$, facing the penetrated Bi melt, slowly reacted with the Bi melt, resulting in 3Dbp-carbon with relatively low porosity (Fig. 1(b)) by boundary diffusion.

The XRD patterns shown in Fig. 2(a) indicate that 3Dbp-carbon became more ordered with increasing graphitization

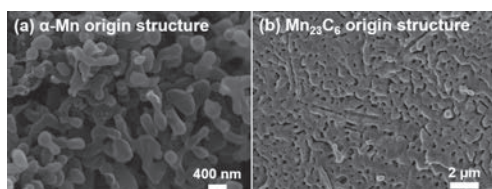


Fig. 1 SEM images of the original (a) α -Mn and (b) $Mn_{23}C_6$ structures of 3D bicontinuous porous carbon prepared by immersing a precursor of $Mn_{85}C_{15}$ (at%) in a pure Bi melt at 1073 K.

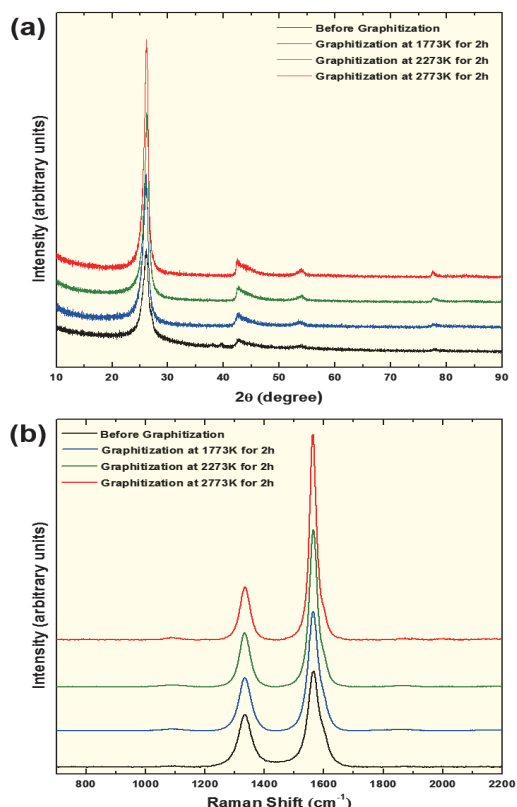


Fig. 2 Comparison of the (a) XRD patterns and (b) Raman spectra before and after graphitization at different temperatures for 2 h.

temperature. The full width at half maximum (FWHM) and lattice spacing for the (002) plane (d_{002}) decreased with increasing graphitization temperature. FWHM_G and the intensity ratio of the D band to the G band decreased with increasing graphitization temperature, as shown in Fig. 2(b). The surface area of 3Dbp-carbon moderately decreased during graphitization at 2773 K. Nevertheless, the total pore volume was almost the same value (~ 0.8 cm³/g) as that under other graphitization conditions. This indicates that the porous structure of the graphitic carbon generated by this dealloying technique is stable during high-temperature graphitization.

References

- [1] SG. Yu, K. Yubuta, T. Wada, and H. Kato, Carbon **96**, 403 (2016).
- [2] T. Wada, K. Yubuta, A. Inoue, and H. Kato, Mater. Lett. **65**, 1076 (2011).

Keywords: foam, porosity, energy storage
Hidemi Kato (Non-Equilibrium Materials Division)
E-mail: hikato@imr.tohoku.ac.jp
URL: <http://www.nem.imr.tohoku.ac.jp/>

Strategy for Obtaining Further Hydrogen-rich Materials

The recent discovery of the highest superconductivity in the sulfur hydride system has stimulated rapidly growing interest in exploring hydrogen-rich materials. Here, we present a strategy for obtaining novel complex transition-metal hydrides containing high-H-coordination hydride complexes.

Hydrogen, in spite of being the simplest element, exhibits an exceptionally rich chemistry, forming various types of chemical bonds in materials. This chemical flexibility is the source of many interesting properties of hydrides, such as hydrogen storage, fast ionic conductivity, magnetism, and metal–insulator transitions [1]. Especially, the recent discovery of superconductivity at 203 K in the sulfur hydride system [2] has spurred research in terms of the exploration of hydrogen-rich materials.

Complex transition-metal hydrides are a typical class of hydrogen-rich materials. In these hydrides, a number of H atoms covalently bond to transition metals to form a varied set of homoleptic transition-metal hydride complexes with a remarkably rich variety of H coordination modes. At the same time, despite research spanning the past several decades, the presently known transition metals capable of forming such complexes are limited to Groups 7–12.

By means of a combined theoretical and experimental approach, we recently demonstrated the formation of the first Group 6 hydride complex

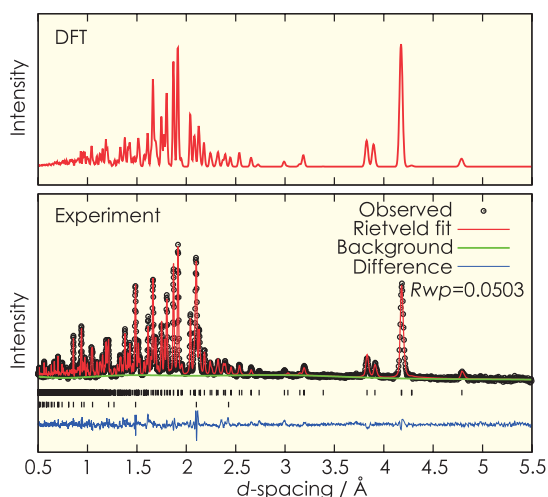


Fig. 1 Neutron diffraction profiles of Mg_3CrH_8 . Simulated profile from DFT structure (top) and experimental profile (bottom).

$[\text{CrH}_7]^{5-}$ in Mg_3CrH_8 [3]. Our density functional theory (DFT) calculations predict that pentagonal-bipyramidal ligand-field allows the formation of strong σ -bonds between H and Cr, thus stabilizing the hydride complex with seven-fold H coordination. The prediction is strongly supported by neutron diffraction (Fig. 1) and infrared (IR) spectroscopic measurements.

In general, the H coordination number increases when going from right to left along a period primarily because of the increase in atomic size, which allows more H atoms to bond (Fig. 2). Thus, our findings strongly suggest high potential for further discovery of hydride complexes with higher H coordination of the unexplored Group 3–6 elements.

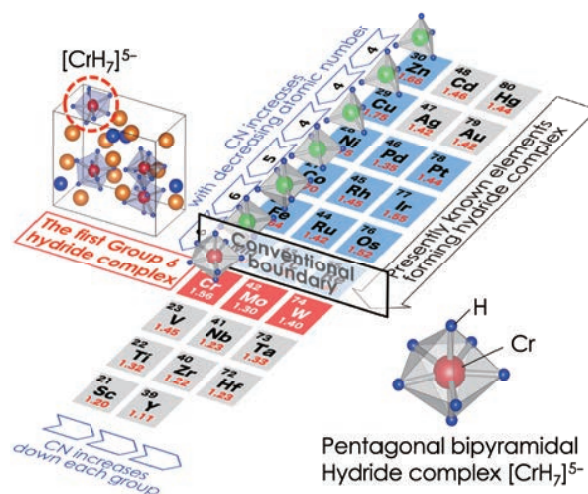


Fig. 2 Schematic of strategy for obtaining hydride complexes with high H coordination.

References

- [1] S. Takagi and S. Orimo, *Scripta Mater.* (Viewpoint paper) **109**, 1 (2015).
- [2] A. P. Drozdov, M. I. Erements, I. A. Troyan, V. Ksenofontov, and S. I. Shylin, *Nature* **525**, 73 (2015).
- [3] S. Takagi, Y. Iijima, T. Sato, H. Saitoh, K. Ikeda, T. Otomo, K. Miwa, T. Ikeshoji, K. Aoki, and S. Orimo, *Angew. Chem. Int. Ed.* **54**, 5650 (2015).

Keywords: hydride, first-principles calculations, crystal structure

Shigeyuki Takagi and Shin-ichi Orimo (Hydrogen Functional Materials Division)

E-mail: shigeyuki.takagi@imr.tohoku.ac.jp

URL: <http://www.hydrogen.imr.tohoku.ac.jp/>

Electronic Materials

IMR KINKEN Research Highlights 2016 

Antiferromagnetic Skyrmions

Topological spin textures such as skyrmions have been actively studied in ferromagnets over the past several years as they may become bits of information in future spintronic memory devices. We propose to study similar topological objects in antiferromagnets, in which the topology and the presence of two sublattices have a large effect on the dynamical and thermal properties.

Manipulating spin textures by electric and spin currents is one of the main challenges in the field of spintronics. Ferromagnetic skyrmions are attracting a lot of attention because they are small and not pinned as easily as domain walls when driven by electric currents. However, ferromagnetic skyrmions have disadvantages as well, such as the presence of stray fields and transverse motion, making it more difficult to employ them in spintronic devices. In this work, we propose a novel topological object, antiferromagnetic (AFM) skyrmion, and we explore its properties analytically and by micromagnetic simulations. This topological texture has no stray fields, as shown in Figs. 1(a) and (b), and it is more mobile than its ferromagnetic analogue.

We found that the Dzyaloshinskii–Moriya interaction, which comes from relativistic spin-orbit effects and generally favors spin spiral structures, stabilizes the AFM skyrmions. The AFM skyrmion radius depends on the strength of the Dzyaloshinskii–Moriya interaction and temperature. Moreover, the thermal properties, such as the radius and diffusion constant, differ from those of ferromagnetic skyrmions. Because of the unusual topology, the AFM skyrmions do not experience a transverse (Magnus) force and therefore do not move transverse to an applied current [Fig. 1(c)], which makes them interesting candidates for spintronic applications [1]. These results can be understood in terms of a generalized Thiele equation, which describes soft modes of the skyrmion motion. This equation shows an exact cancelation of the Magnus force due to the presence of two AFM sublattices with opposite topological charges. It also leads to a larger diffusion constant of the AFM skyrmion as compared to its ferromagnetic counterpart.

The next step will be to investigate the efficiency of temperature gradients for the propagation of skyrmions in antiferromagnetic insulators and to develop a theory of spin-orbit torque driven AFM skyrmion motion in AFM/heavy metal bilayers.

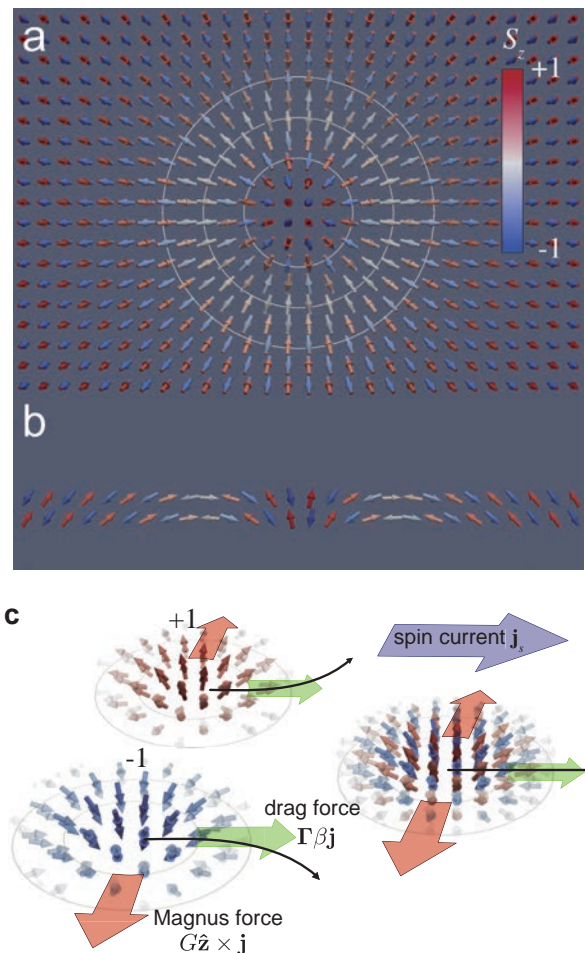


Fig. 1 (a)–(b) The spin texture of an antiferromagnetic (AFM) skyrmion: (a) top view of the AFM skyrmion and (b) skyrmion's cross section. (c) The AFM skyrmion is a composite topological object consisting of a skyrmion on one sublattice and an antiskyrmion on the other. This results in the cancelation of the overall Magnus force and therefore the absence of the topological Hall effect.

References

- [1] J. Barker and O. A. Tretiakov, Phys. Rev. Lett. **116**, 147203 (2016)

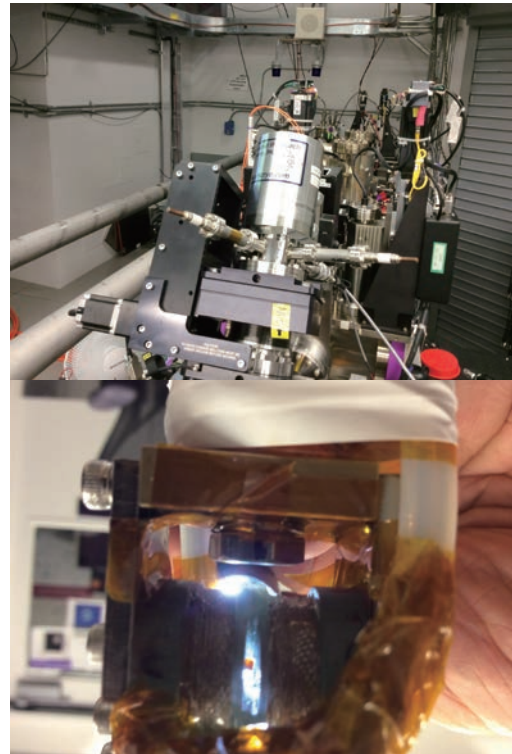
Fusion of Pulse Fields and Pulse X-ray Unveils New Charge Density Wave State

Development of a three-dimensional correlation of a charge density wave in $\text{YBa}_2\text{Cu}_3\text{O}_{6.67}$ was discovered by single-shot X-ray diffraction in high magnetic fields. The combination of the pulsed magnet and the intense pulse X-ray enabled us to pick up the extremely weak super-lattice modulation caused by the magnetic field-induced electronic phase transition.

High magnetic fields induce various electronic phase transitions such as metal-insulator, charge density wave (CDW), and valence-state transitions. Unique structural anomalies are associated with these transitions, but observations of such tiny changes of crystal symmetry and/or volume have been difficult. For example, CDW states appearing under high magnetic fields in Cu oxide superconductors have been intensively studied. However, direct observation of a CDW super-lattice peak has been made only in magnetic fields much lower than the upper critical fields. An ultimate tool to investigate such small lattice modulations in extremely high magnetic fields had been sought for long time.

In the current study, we combined two pulsed tools, a pulsed magnet and a pulsed X-ray source, to accomplish this difficult task. The magnetism division of IMR has developed an extremely compact split-pair magnet generating magnetic fields of over 30 T. The bore of the coil is only 3 mm and the length of the coil is as short as 25 mm. The SLAC National Accelerator Laboratory offers the most intense pulsed laser source on earth. When these two tools are combined, weak CDW peaks in $\text{YBa}_2\text{Cu}_3\text{O}_{6.67}$ can be detected clearly in a single-shot pulsed magnetic field [1]. It should be also noted that IMR offers a compact capacitor bank developed and assembled at the magnetism division. The “flying magnet” and the “rolling capacitor bank” make this fusion possible.

In the present experiments, a new CDW state with strong three-dimensional correlation was discovered. The index of this CDW state is given by $(\delta, 0, l)$, where δ is related to the localized charge modulation in the c -plane. Moreover, the index l was found to be an integer. This unique feature is in sharp contrast to the two-dimensional CDW peak found in lower magnetic fields at the $(\delta, 0, l/2)$ position, where the modulation pitch along the c -axis is doubled. The intensity of the $l = \text{integer}$ peak increased rapidly in high magnetic fields, whereas that of the half-integer peak saturated in lower magnetic fields. The appearance of a state with localized electrons with such strong three-



The figure shows the X-ray diffraction chamber used at Linac Coherent Light Source at SLAC National Accelerator Laboratory for a single-shot high-magnetic-field X-ray diffraction and the split-pair pulse coil mounted on the cold finger of the specimen.

dimensionality shows the essential role of the strong electron correlation in the normal state of $\text{YBa}_2\text{Cu}_3\text{O}_{6.67}$ and the existence of a few competing interactions. The present experiment demonstrates the power of the new tool for investigating magnetic field-induced electronic transitions.

References

- [1] S. Gerber, H. Jang, H. Nojiri, S. Matsuzawa, H. Yasumura, D. A. Bonn, R. Liang, W. N. Hardy, Z. Islam, A. Mehta, S. Song, M. Sikorski, D. Stefanescu, Y. Feng, S. A. Kivelson, T. P. Devereaux, Z.-X. Shen, C.-C. Kao, W.-S. Lee, D. Zhu, and J.-S. Lee, *Science* **350**, 949 (2015).

Keywords: high magnetic field, superconducting, X-ray scattering
 Hiroyuki Nojiri (Magnetism Division)
 E-mail: nojiri@imr.tohoku.ac.jp
 URL: <http://www.hfpm.imr.tohoku.ac.jp/>

Fluid-mechanical Spin-current Generation

Fundamental studies of spintronics focus on the manipulation and generation of spin currents. To generate spin currents, recent studies have utilized several interactions with electron spins in condensed matter; the key is angular momentum conversion. Here, we experimentally show that fluid-mechanical angular momentum enables us to generate spin currents.

Macroscopic mechanical rotation is the most common carrier of angular momentum. Mechanical rotation can interact with electron spins directly, as suggested by the Barnett effect, inducing spin polarization by mechanical rotation of a material object. However, generation of a spin current as a result of mechanical rotation has not been observed so far because it requires a mechanical rotation gradient, and producing such a rotation gradient is difficult in a solid. However, in fluid motion, and even in a conventional liquid flow in a pipe, we can easily generate mechanical rotation by using the vorticity, which is the local rotation of a liquid due to the viscosity near the inner wall [Fig. 1(a)]. Hence, as the liquid flows through the pipe, a spin current due to macroscopic motion is expected to be generated along the direction of the vorticity gradient, perpendicular to the pipe flow.

In the present study [1], to detect the spin current in a liquid, especially liquid metals (such as Hg and the gallium alloy $\text{Ga}_{62}\text{In}_{25}\text{Sn}_{13}$), we used the inverse spin Hall (ISH) effect, converting a spin current into electric voltage perpendicular to the spin-current direction through the spin-orbit interaction of electrons. Hence, in the pipe flow, the ISH voltage is expected to be generated along the flow direction [Fig. 1(a)]. Figure 1(b) shows the results of measurements of the voltage along the flow direction in the Hg pipe flow. A clear voltage signal appears when Hg is flowing. The sign of the signal is reversed upon reversing the flow direction; this unconventional voltage behavior is predicted for the ISH effect induced by the mechanical motion described above. We also examined the consistency of the current results with the theory on spin-current generation due to fluid motion [1].

This phenomenon is fundamentally new; it bridges the gap between spintronics and hydrodynamics, and it is expected to become a stepping-stone to expanding spintronic phenomena into fluids.

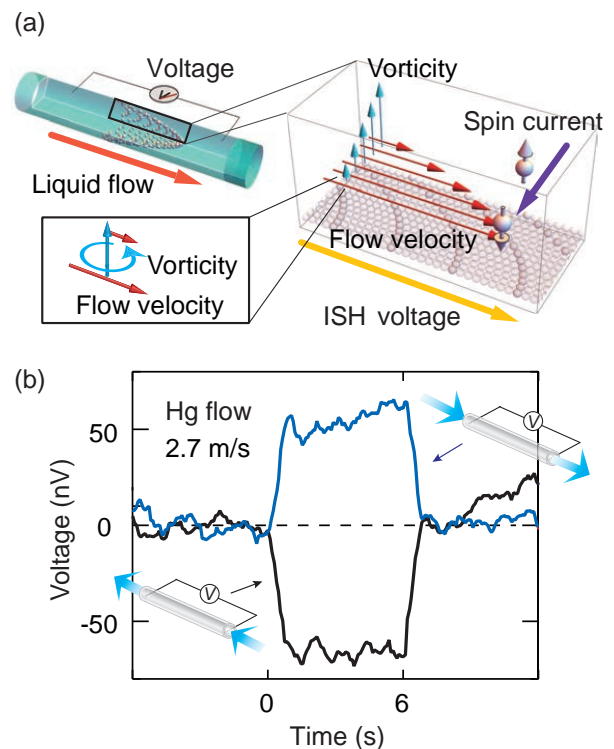


Fig. 1 (a) Concept of fluid-mechanical spin-current generation. Translational motion with different velocities in a local flow region exhibits local rotational motion whose angular velocity is proportional to the vorticity. The vorticity gradient becomes a spin-current source. (b) Time evolution of voltage signals induced by the Hg flow. The flow was started at 0 s and switched off at 6 s. The length and inner diameter of the pipe were 80 mm and 0.4 mm, respectively. The measurements were performed at room temperature.

References

- [1] R. Takahashi, M. Matsuo, M. Ono, K. Harii, H. Chudo, S. Okayasu, J. Ieda, S. Takahashi, S. Maekawa, and E. Saitoh, *Nature Phys.* **12**, 52 (2016).

High- T_c Superconductivity of FeSe Emerges in Thinning Manner

Two-dimensional layered materials possess significant potential to exhibit intriguing physical properties by combining external electric fields. Iron selenide (FeSe) is a layered material that has received much attention because of its high superconducting transition temperature (high- T_c) when an atomic monolayer is deposited onto SrTiO₃. Here, we highlight a new approach to obtaining high- T_c superconductivity of ultrathin FeSe films by an electrochemical reaction in an electric double-layer transistor (EDLT). The EDLT allows layer-by-layer electrochemical etching of FeSe films down to an atomic monolayer and electrostatic control of the superconductivity.

FeSe is an iron-based superconductor with a superconducting transition temperature (T_c) of 8 K in bulk form [1]. Stacking of Se–Fe–Se atoms forms a layered crystal structure. The recent astonishing discovery of its high- T_c superconductivity with a large gap of approximately 20 meV corresponding to $T_c = 65$ K has sparked an explosion of investigations of atomic monolayers of FeSe deposited onto SrTiO₃ substrates by mainly *in-situ* characterization using photo-emission and scanning tunneling spectroscopies [2, 3]. However, the systematic thickness dependence of electrical measurements of the superconductivity and its electric field effect have not been addressed so far, mainly because of the experimental difficulty in obtaining *ex-situ* measurements for atomically thin films.

To overcome this issue, we applied the electric double-layer transistor (EDLT) technique with thick FeSe films grown by pulsed-laser deposition [4]. EDLTs were originally employed to investigate novel physical phenomena with significant charge carrier accumulation. Our team applied the EDLT technique to regulate the FeSe film thickness by an electrochemical reaction, enabling layer-by-layer etching down to an atomic monolayer. With decreasing thickness, a high- T_c superconductivity of 40 K surprisingly emerged in *ex-situ* electrical resistivity measurements (brown curve in Fig. 1). In addition, the systematic thickness dependence of the superconductivity was successfully revealed in our study. Moreover, electrical control of the superconductor-to-insulator transition was realized via control of the external electric field (from the red to the purple curves in Fig. 1). Our results point out the importance of electric-field-induced electronic band modulation for generating high- T_c superconductivity in FeSe.

This electrochemical etching approach could be applied to other layered materials. We believe this method is a powerful technique for exploring novel physical phenomena in two-dimensional layered systems.

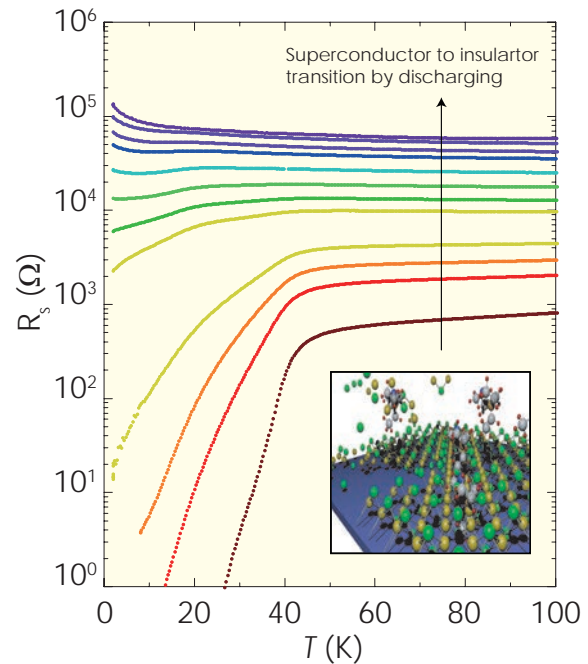


Fig. 1 Superconducting transition behavior in EDLT device upon applying an external electric field (brown curve). A decrease in the number of charge carriers (discharging) induced superconductor-to-insulator transition (from red to purple). (Inset) Schematic image of atomic layer of FeSe in ionic liquid.

References

- [1] F. C. Hsu, J. Y. Luo, K. W. Yeh, T. K. Chen, T. W. Huang, P. M. Wu, Y. C. Lee, Y. L. Huang, Y. Y. Chu, D. C. Yan, and M. K. Wu, *Proc. Natl. Acad. Sci. USA* **105**, 14262 (2008).
- [2] Q. Y. Wang, Z. Li, W. H. Zhang, Z. C. Zhang, J. S. Zhang, W. Li, H. Ding, Y. B. Ou, P. Deng, K. Chang, J. Wen, C. L. Song, K. He, J. F. Jia, S. H. Ji, Y. Y. Wang, L. L. Wang, X. Chen, X. C. Ma, and Q. K. Xue, *Chin. Phys. Lett.* **29**, 037402 (2012).
- [3] S. He, J. He, W. Zhang, L. Zhao, D. Liu, X. Liu, D. Mou, Y. B. Ou, Q. Y. Wang, Z. Li, L. Wang, Y. Peng, Y. Liu, C. Chen, L. Yu, G. Liu, X. Dong, J. Zhang, C. Chen, Z. Xu, X. Chen, X. Ma, Q. Xue, and X. J. Zhou, *Nature Mater.* **12**, 605 (2013).
- [4] J. Shiogai, Y. Ito, T. Mitsuhashi, T. Nojima, and A. Tsukazaki, *Nature Phys.* **12**, 42 (2016).

Keywords: superconducting, thin films, field-effect transistor
 Junichi Shiogai (Low Temperature Physics Division)
 E-mail: junichi.shiogai@imr.tohoku.ac.jp
 URL: http://mu.imr.tohoku.ac.jp/index_en.html

Charge Degrees of Freedom under High Pressure in the Organic Dimer-Mott Insulator β' -(BEDT-TTF) $_2$ Cl $_2$

Low-dimensional layered organic conductors are a promising class of materials that exhibit high-temperature superconductivity. Among them, an antiferromagnetic dimer-Mott insulator, β' -(BEDT-TTF) $_2$ Cl $_2$, showed superconductivity at 14.2 K under 8 GPa. We performed optical conductivity measurements for β' -(BEDT-TTF) $_2$ Cl $_2$ under high pressure, which revealed that charge fluctuations inside dimers play an important role in high-temperature superconductivity.

The organic conductor β' -(BEDT-TTF) $_2$ Cl $_2$, which shows superconductivity at 14.2 K under high pressure (~ 8 GPa), has aroused significant interest because its transition temperature is the highest among organic superconductors known to date. At ambient pressure, β' -(BEDT-TTF) $_2$ Cl $_2$ is a dimer-Mott (DM) insulator with an antiferromagnetic transition temperature, T_N , of 22 K. As typically seen in bandwidth-controlled Mott transition systems, β' -(BEDT-TTF) $_2$ Cl $_2$ also exhibits superconductivity when the antiferromagnetic phase is suppressed by applying pressure. It is believed, therefore, that antiferromagnetic spin fluctuations play an essential role in high- T_c superconductivity.

To elucidate the effect of pressure on the superconductivity of β' -(BEDT-TTF) $_2$ Cl $_2$, we measured the polarized infrared (IR) optical spectra under high pressure using a diamond anvil cell (DAC) [Fig. 1(a)] [1]. At ambient pressure, two characteristic bands due to intra- and interdimer charge transfers were observed in the IR spectra, indicating that this salt is a typical half-filled DM insulator at ambient pressure [Fig. 1(b)]. With increasing pressure, however, the intradimer charge transfer excitation shifted to much lower energies, indicating that the effective electronic state changes from half-filled to three-quarters-filled as a result of weakening of dimerization [Fig. 1(c)]. This implies that the system approaches a charge-ordered state under high pressure, in which charge degrees of freedom emerge as an important factor. The present results suggest that in addition to antiferromagnetic spin fluctuations, charge fluctuations inside dimers play an important role in high-temperature superconductivity.

References

- [1] K. Hashimoto, R. Kobayashi, H. Okamura, H. Taniguchi, Y. Ikemoto, T. Moriwaki, S. Iguchi, M. Naka, S. Ishihara, and T. Sasaki, *Phys. Rev. B* **92**, 085149 (2015).

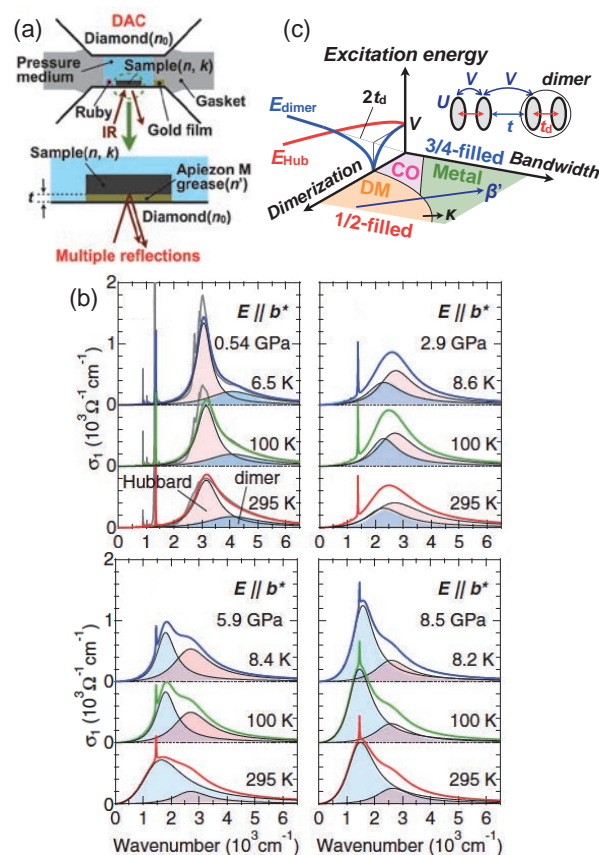


Fig. 1 (a) Experimental setup for the optical measurements under high pressure using a DAC. (b) Optical conductivity spectra of β' -(BEDT-TTF) $_2$ Cl $_2$ measured in the DAC at various pressures. The gray lines in the upper left panel show the $\sigma_1(\omega)$ spectra measured at ambient pressure. (c) The schematic phase diagram expected in the extended Hubbard model with the molecular dimer degree of freedom is shown as functions of degree of dimerization and bandwidth. The excitation energies of the Hubbard and dimer bands are also shown as functions of degree of dimerization. In β' -(BEDT-TTF) $_2$ Cl $_2$, when the pressure is applied, the system would follow the track drawn by the arrow.

Keywords: organic, superconducting, optical properties
 Kenichiro Hashimoto (Low Temperature Condensed State Physics Division)
 E-mail: hashimoto@imr.tohoku.ac.jp
 URL: <http://cond-phys.imr.tohoku.ac.jp/index.html>

Spin Fluctuations on a Triangular Lattice

In geometrically frustrated magnets, *spin liquid* states attract considerable interest. We quantitatively examined temporal magnetic correlations of the triangular lattice antiferromagnet NiGa₂S₄ through thirteen decades (10⁻¹³–1 s) and elucidated that megahertz spin fluctuations last over an extended temperature regime.

Two-dimensional triangular lattices play a prominent role in the field of frustrated magnetism. Although it now seems clear that a conventional triangular lattice antiferromagnet has a long-range 120-deg order, irrespective of the spin quantum number, S , experiments on materials with generalized longer-range and spin-orbit interactions, as well as lattice distortions, point to a rich variety of phases in the vicinity of the ordered phase. In the quantum limit ($S = 1/2$) first considered by Anderson, experiments on organic materials suggested that a gapless spin liquid with a spinon Fermi surface may exist near the metal–insulator transition.

For larger spin quantum numbers, theoretical and experimental works have pointed to complex slow spin dynamics that are still poorly understood. Here, we focus on such dynamics in the $S = 1$ triangular lattice antiferromagnet NiGa₂S₄, which is distinguished by a two-dimensional incommensurate magnetic wave vector and the potential for spin-nematic interactions.

NiGa₂S₄ consists of neutral insulating layers held together by van der Waals forces [inset to Fig. 1(a)]. This curtails electron hopping between layers and leads to a strongly two-dimensional magnet. Within each layer, nickel ions with $S = 1$ reside on an equilateral triangular lattice. Upholding expectations of anomalous magnetism, the material does not exhibit conventional magnetic ordering down to a temperature T of 50 mK, and the in-plane correlation length gradually increases upon cooling but tends to remain at approximately 2.6 nm (7 lattice spacings) without a thermal anomaly [Fig. 1(a)].

In sharp contrast, *temporal* correlations feature clear thermal anomalies. Figure 1(b) shows the temperature dependence of the characteristic spin relaxation time in NiGa₂S₄. Using high-energy resolution inelastic neutron scattering, neutron spin echo, muon spin relaxation, and AC magnetometry, we provide evidence for emergent MHz spin dynamics over a wide range of temperatures [1]. We argue that such slow spin dynamics are associated with emergent topologically protected degrees of freedom inherent to incommensurate magnetism on

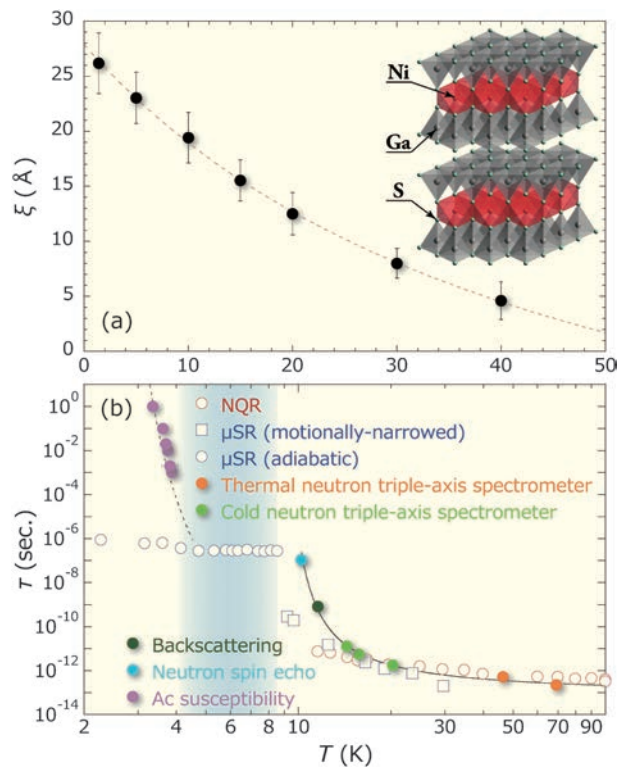


Fig. 1 Temperature dependence of (a) the spin correlation length and (b) characteristic spin relaxation time of NiGa₂S₄. The crystal structure of NiGa₂S₄ is depicted in the inset to (a). Above and below $T^* = 8.5$ K, the muon spin relaxation rates are in the motionally narrowed and adiabatic limits, respectively. Vogel–Fulcher behavior from the AC susceptibility measurements is given by the dotted curve. The dashed curve in (a) and the solid curve towards T^* in (b) are visual guides.

the triangular lattice.

References

- [1] Y. Nambu, J.S. Gardner, D.E. MacLaughlin, C. Stock, H. Endo, S. Jonas, T.J. Sato, S. Nakatsuji, and C. Broholm Phys. Rev. Lett. **115**, 127202 (2015).

Keywords: neutron scattering, triangular antiferromagnet, spin fluctuation
 Yusuke Nambu (Metal Physics with Quantum Beam Spectroscopy Division)
 E-mail: nambu@imr.tohoku.ac.jp
 URL: <http://qblab.imr.tohoku.ac.jp/>

Dislocation-based Plasticity of Si

The classical idea that semiconductor silicon (Si) is brittle and cannot be deformed plastically at room temperature (RT) is now changing drastically. Recent experimental findings on the plasticity of Si from RT to its melting temperature (T_m) in terms of dislocation mobility and atomic core structure are reviewed.

Si is a key material in nano-sized devices for ultra-large-scale integrated (ULSI) circuits and for precision instruments for micro-electromechanical systems (MEMS). Knowledge of the elastic–plastic characteristics of Si is essential for controlling its crystallinity during various fabrication processes. Si is known to be typically ductile at temperatures higher than approximately $2/3T_m$, behavior that is governed by dislocation dynamics, whereas at lower temperatures, Si is brittle and susceptible to fracture without plastic deformation owing to the extremely low mobility of dislocations. Thus, there is a ductile-to-brittle transition (T_{DBT}) in the deformation mode at approximately 600–700°C.

Figure 1 shows the mechanical strength of Si crystals plotted against the reciprocal temperature from RT to 1300°C [1]. There are two regions with remarkable knees at approximately 400°C, showing a drastic change in the temperature dependence of the strength. At temperatures higher than the knees, Si deformed by compression or tension under atmospheric pressure, being ductile in conventional viewpoints. Surprisingly, Si deforms plastically even at temperatures from RT to the knee under specially arranged conditions. Small, thin plates (membranes) or micro-scale pillars whose thickness and diameter, respectively, are on the order of micrometers, can be deformed by compression or tension at atmospheric pressure. Bulk specimens can be compressively deformed without fracture under a confining (hydrostatic) pressure. Under these conditions, T_{DBT} decreases to temperatures close to RT. In low-temperature regions, the yield strength of Si is as high as 1.5 GPa, almost independent of the temperature, which is extremely different from its behavior at high temperatures. This feature leads to the so-called shuffle–glide controversy on the core structure of dislocations governing the plasticity of Si in the relevant temperature regions.

Plastic deformation of a crystal takes place through the generation, motion, and multiplication of dislocations in the crystal under stress. The processes are controlled by the dynamic properties of the dislocations. The dislocation velocity has

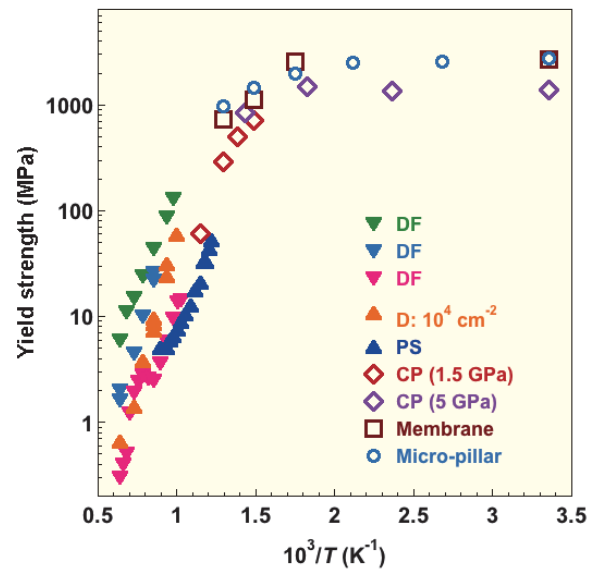


Fig. 1 Temperature dependence of strength of Si under various conditions [1]. DF: dislocation-free, D: dislocated, PS: pre-strained, CP: under confining pressure.

been well determined experimentally as a function of stress and temperature.

At high temperatures, the deformation processes are governed by the dynamic collective motion of glide-set dislocations. The process can be reproduced by the constitutive model with mutual interaction and self-multiplication of dislocations [2]. On the other hand, the generation of shuffle-set dislocations is favorable in deformation at the temperatures under the application of extremely high stress.

References

- [1] I. Yonenaga, Eng. Fracture Mechanics **147**, 468 (2015).
- [2] J. Cochard, I. Yonenaga, M. M'Hamdi, and Z. L. Zhang, J. Mech. Phys. Sol. **61**, 2402 (2014).

Keywords: defects, deformation, semiconducting
 Ichiro Yonenaga (Physics of Crystal Defects Division)
 E-mail: yonenaga@imr.tohoku.ac.jp
 URL: <http://lab-defects.imr.tohoku.ac.jp/>

Measurement of Internal Electric Fields in Group-III Nitride Devices by Electroreflectance Spectroscopy

Nitride semiconductor-based devices have strong polarization-induced internal electric fields, which affect the device performance. To improve the device performance, it is important to design a device structure that takes the actual internal electric fields into consideration. In this study, the internal electric field was directly measured by electroreflectance spectroscopy.

Group-III nitride semiconductors exhibit a wurtzite crystal structure, and they have crystallographic polarity as a result of this crystal structure. The choice of crystallographic polarity is one of the key issues because it influences several properties in terms of the crystal growth and device characteristics. N-polar growth facilitates the growth of InGaN with a high InN-molar fraction. In a previous study, N-polar InGaN/GaN light-emitting diodes (LEDs) operating across the visible spectrum have been demonstrated [1].

Devices based on group-III nitride semiconductors often have polarization-induced electric fields, which affect device performance [2, 3]. In order to realize high-efficiency devices, the device structure has to be designed by taking into consideration the actual internal electric fields induced by the crystallographic polarization. Up to now, there has been no report on the direct measurement of such fields. In this study, electroreflectance (ER) spectroscopy was adopted to investigate the actual internal electric fields in III-polar and N-polar InGaN/GaN LEDs. A comparable study for LEDs fabricated on GaN with different crystal orientation is thus demonstrated for the first time.

In ER measurements, the phases of the ER spectra are affected with the direction of the internal electric fields. Schematic diagrams of the energy band profiles and dielectric constants for III-polar and N-polar InGaN/GaN quantum wells are shown in Fig. 1. In InGaN layers with different polarities, the directions of the built-in electric fields are opposite each other. Therefore, the phase of an ER signal will be different depending on the direction of the internal electric fields. Figure 2 shows the ER spectra for III-polar and N-polar LEDs. The phases of the ER signals from the InGaN layers were opposite each other in the III-polar and N-polar samples. By fitting the ER spectra, the internal electric fields were estimated to be +2.3 MV/cm and -1.1 MV/cm for N-polar and III-polar LEDs, respectively. In conclusion, ER spectroscopy is confirmed as an effective method to directly measure the actual internal electric fields.

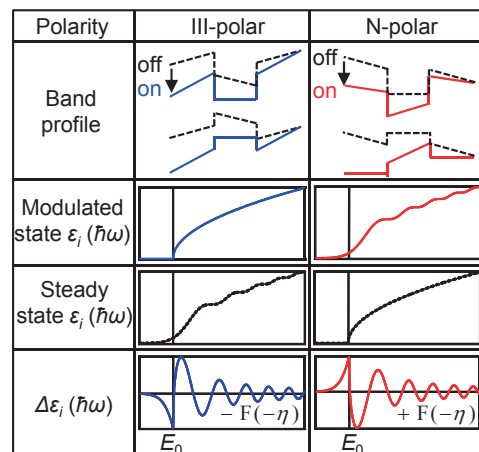


Fig. 1 Schematic diagrams of energy band profiles and difference between the steady-state and the modulated state in the imaginary part of dielectric constants $\epsilon_i(\hbar\omega)$.

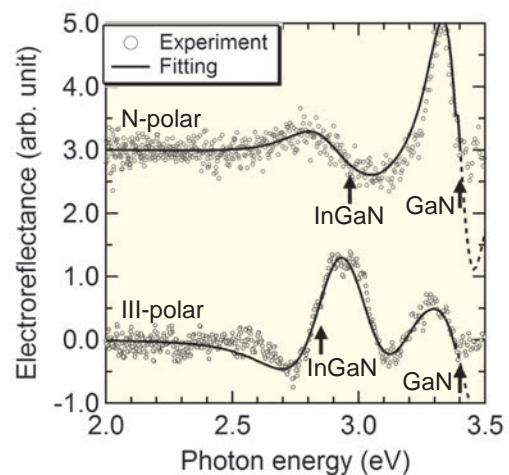


Fig. 2 ER spectra for III-polar and N-polar InGaN/GaN MQW-LEDs.

References

- [1] K. Shojiki, T. Tanikawa, J. H. Choi, S. Kuboya, T. Hanada, R. Katayama, and T. Matsuoka, *Appl. Phys. Express* **8**, 061005 (2015).
- [2] T. Aoki, T. Tanikawa, R. Katayama, T. Matsuoka, and K. Shiojima, *Jpn. J. Appl. Phys.* **55**, 04EJ09 (2016).
- [3] T. Tanikawa, K. Shojiki, R. Katayama, S. Kuboya, and T. Matsuoka, *Jpn. J. Appl. Phys.* **55**, 05FJ03 (2016).

Keywords: crystal growth, optoelectronic, spectroscopy
 Takashi Matsuoka (Physics of Electronic Materials Division)
 E-mail: matsuoka@imr.tohoku.ac.jp
 URL: <http://www.matsuoka-lab.imr.tohoku.ac.jp/?TOPPAGE>

Design of Rigid Molecular Magnetic Frameworks from a Combination of Chain and Layer

The design of three-dimensional (3D) magnetic pathways is a crucial point for the creation of molecular magnets. We have recently reported a new strategy for constructing 3D magnetic frameworks: π -type donor molecules, which could make a magnetic pathway, could be combined with π -type acceptor magnetic layers. This framework was named “ π -stacked pillared layer frameworks” (π -stacked PLFs). In this framework, we can integrate a magnetic pathway, even in the inter-layer direction, through inserted paramagnetic molecules.

Layered magnetic frameworks, which are often producible in the synthesis of molecular magnets, are useful for designing hybrid materials with new functional molecules intercalated between layers; however, are disadvantage to creating high T_c magnets. We previously reported a new class of molecular magnets made from a D₂A formulation of paramagnetic electron-donor (D) units (paddlewheel-type diruthenium(II, II) unit; [Ru₂^{II,II}]) and electron-acceptor (A) units (tetracyano-*p*-quinodimethane derivatives; TCNQ_{*x*}) [1]. This type of compound mainly provided layered magnets, which made it difficult to control inter-layer interactions [2].

Here, we introduce a unique three-dimensional framework named a “ π -stacked pillared layer framework (π -stacked PLF)” for magnet design. Two types of low-dimensional magnet frameworks, a D₂A magnetic layer noted above and a charge transfer [FeCp*₂]⁺TCNQ^{•-} columnar magnet ([FeCp*₂]⁺ = decamethylferrocenium), were integrated in order to fabricate the magnet [3]. [FeCp*₂]⁺TCNQ^{•-} was reported by Miller et al. and is known to form a π -stacking alternating column comprising ferromagnetically coupled Coulombic sets [FeCp*₂]⁺ and TCNQ^{•-} with $S = \frac{1}{2}$ [4]. When combined with the layered D₂A, the [FeCp*₂]⁺ unit acts as a π -stacking pillar for the D₂A layers sandwiched between TCNQ^{•-} moieties, resulting in a π -stacking PLF with the formula [FeCp*₂][Ru₂TCNQ] (Fig. 1).

The π -stacked PLF compound exhibited a ferrimagnetic phase transition at 82 K (Fig. 1), which could be increased to 107 K by applying a pressure of 12.5 kbar. These results imply that the inserted spin of [FeCp*₂]⁺ affected the formation of the three-dimensional spin arrangement. This synthetic strategy employing a combination of layers and chains is widely useful for magnet design based on molecular assemblies.

References

[1] H. Miyasaka, *Acc. Chem. Res.* **46**, 248 (2013).

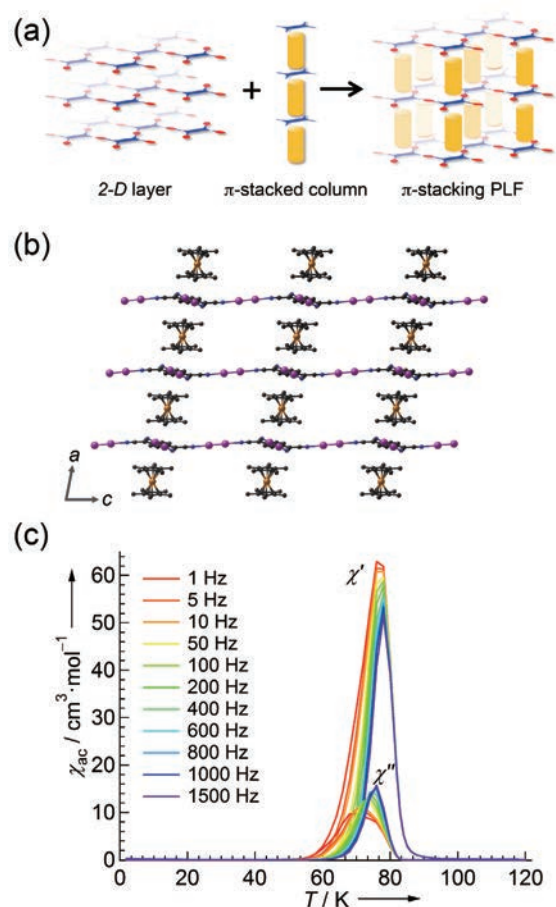


Fig. 1 (a) Schematic representation of the design strategy for π -stacked PLF. (b) The layered structure of the obtained π -stacked PLF compound. (c) Temperature-dependence of ac susceptibilities (in-phase χ' and out-of-phase χ'') of the compound.

[2] H. Miyasaka, T. Izawa, N. Takahashi, M. Yamashita, and K. R. Dunbar, *J. Am. Chem. Soc.* **128**, 11358 (2006).

[3] H. Fukunaga and H. Miyasaka, *Angew. Chem. Int. Ed.* **54**, 569 (2015).

[4] G. A. Candela, L. J. Swartzendruber, J. S. Miller, and M. J. Rice, *J. Am. Chem. Soc.* **101**, 2755 (1979).

Keywords: magnetic properties, crystal structure, ferromagnetic
Hitoshi Miyasaka (Solid-State Metal-Complex Chemistry Division)
E-mail: miyasaka@imr.tohoku.ac.jp
URL: <http://www.miyasaka-lab.imr.tohoku.ac.jp/>

Enhanced Output of the Giant Magnetoresistance Junction for Hard Disc Drive Applications

Current perpendicular to plane giant magnetoresistance (CPP-GMR) junctions are a key element for future reading head applications of hard disk drives with an areal recording density of several tera-bit per square inches, which is being demanded for storing the enormous amount of data present in society. We succeeded in enhancing the device output of the CPP-GMR junctions using half-metallic Heusler alloy electrodes and a newly developed Ag-Mg alloy spacer material.

In the last decade, there has been a drastic increase in the amount of information handled by society. Hard disc drives (HDDs) are one of the major storage devices with high data retention and low cost. It is necessary to develop HDDs of several tera-bit per square inches areal density for supporting this information. Toward this aim, it is necessary to enhance the sensitivity of the reading head devices. The current perpendicular-to-plane giant magnetoresistance (CPP-GMR) junction is expected to have useful applications in future HDDs [1]. It has been demonstrated that CPP-GMR junctions using half-metallic cobalt (Co)-based Heusler alloys and a silver (Ag) spacer layer exhibit a large device output compared with conventional 3d-transition-metal-based junctions [2, 3]. In this work, we have developed a new non-magnetic spacer layer, Ag-Mg alloy, which provides a larger device output than the previously used Ag spacer layer [4].

Figure 1 (a) shows a high-angle annular dark field scanning transmission electron microscope (HAADF-STEM) image of a layered film for the CPP-GMR junction, in which a Ag-Mg spacer layer is sandwiched with $\text{Co}_2(\text{Fe-Mn})\text{Si}$ Heusler alloy electrodes. Epitaxial growth and well-defined interfaces are clearly confirmed by the image. A HAADF-STEM image of a junction used for measuring the CPP-GMR effect is shown in Fig. 1 (b), and it is confirmed that a sub-micrometer-scaled junction was successfully fabricated. A typical result of the CPP-GMR effect is shown in Fig. 2 (a): The resistance of the junction clearly changed depending on the configuration of the magnetizations for the $\text{Co}_2(\text{Fe-Mn})\text{Si}$ electrodes, which is schematically described above the graph. The performance of the junction was characterized by investigating the bias voltage dependence of the output voltage (Fig. 2 (b)). The output of the newly developed Ag-Mg-spacer junction is about 25% larger than that of the conventional Ag-spacer. Our material can contribute to the development of next generation HDD-reading heads.

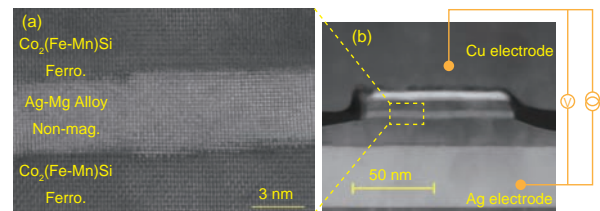


Fig. 1 (a) High-angle annular dark field scanning transmission electron microscope (HAADF-STEM) images of a $\text{Co}_2(\text{Fe-Mn})\text{Si}/\text{Ag-Mg}/\text{Co}_2(\text{Fe-Mn})\text{Si}$ layered film, and (b) a CPP-GMR junction. Copyright (2015) The Japan Society of Applied Physics.

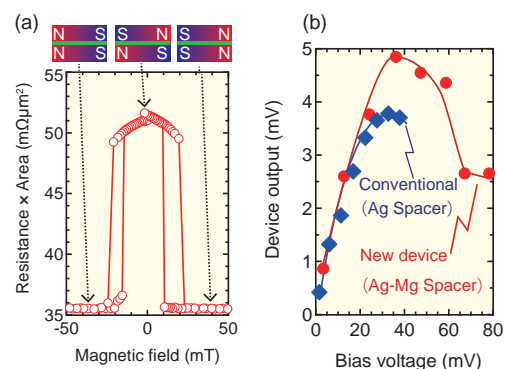


Fig. 2 (a) A CPP-GMR curve of a junction. High resistance state is observed for the anti-parallel magnetization configuration. (b) Device outputs as a function of the applied bias voltage for Ag spacer (diamond) and Ag-Mg spacer (circle) junctions. Copyright (2015) The Japan Society of Applied Physics.

References

- [1] M. Takagishi, K. Yamada, H. Iwasaki, H. N. Fuke, and S. Hashimoto, *IEEE Trans. Magn.* **46**, 2086 (2010).
- [2] Y. Sakuraba, M. Ueda, Y. Miura, K. Sato, S. Bosu, K. Saito, M. Shirai, T. J. Konno, and K. Takanashi, *Appl. Phys. Lett.* **101**, 252408 (2012).
- [3] S. Li, Y. K. Takahashi, T. Furubayashi, and K. Hono, *Appl. Phys. Lett.* **103**, 042405 (2013).
- [4] H. Narisawa, T. Kubota, and K. Takanashi, *Appl. Phys. Express* **8**, 063008 (2015).

Keywords: magnetoresistance, half-metal, spintronics
 Koki Takanashi (Magnetic Materials Division)
 E-mail: koki@imr.tohoku.ac.jp
 URL: <http://magmatelab.imr.tohoku.ac.jp/>

Which Crystal Site Do Impurities Adore?

Crystal sites for impurities in lithium niobates (LN) were revealed by combining lattice constant measurements with thermodynamic constraints. Divalent and trivalent impurities were located at Li sites in LN, whereas tetravalent impurities were located at Nb sites. This result provides good clues for suppressing point defects, which enhances optical application of LN.

Lithium niobate (LiNbO_3 : LN) is a ferroelectric material that shows excellent and versatile properties. LN has therefore been used as a substrate for nonlinear optical devices, as well as for surface acoustic wave devices. LN crystals are normally grown from the congruent melt to obtain a homogeneous composition. Because congruent LN (c-LN) contains more Nb than stoichiometric LN, excess Nb generates intrinsic point defects at Li sites. In the “Li site vacancy model” (Fig. 1) [1], intrinsic defects are antisite Nb (Nb_{Li}) and vacancies (V_{Li}) at Li sites. In particular, Nb_{Li} causes photorefractive damage, which hinders optical application of LN. Regarding this problem, doping impurities such as MgO were found to be effective for increasing the damage threshold [1]. However, it is not fully understood into which site impurities are incorporated and how impurities decrease the Nb_{Li} concentration. Here, the selection of impurity sites and Nb_{Li} behavior in impurity-doped c-LN were investigated by analyzing the defect structures, i.e., configurations of point defects, including impurities and intrinsic defects. The defect structures were determined by lattice constant measurements [2] combined with thermodynamic constraints [3].

Several defect structures of impurity-doped LN are possible depending on the occupancy of the impurities and the intrinsic defects in crystal sites. Among them, unfeasible defect structures can be excluded by considering thermodynamic constraints, that is, by evaluating the degrees of freedom in each crystal site [3]. The degrees of freedom are obtained by subtracting the number of thermodynamic constraints from the number of parameters. The number of parameters at each site corresponds to the number of elements, including defects such as antisite defects and vacancies. Meanwhile, thermodynamic constraints include mass conservation at each site and the element exchange in equilibrium [3]. The thermodynamic analysis revealed that only structures A and B (Fig. 1) are feasible out of the six models.

In structure A, impurities locate at the Li site

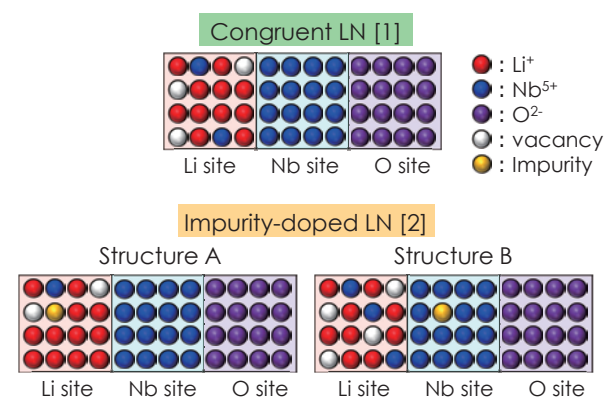


Fig. 1 Defect structures of congruent LN and impurity-doped LN.

where V_{Li} and Nb_{Li} also exist. In structure B, Impurities locate at the Nb site while V_{Li} and Nb_{Li} exist at the Li site.

Because the relationship between impurity concentration and lattice constants for structures A and B differ, the defect structures can be differentiated by analyzing lattice constant variations with impurity concentration. The results show that the defect structure of divalent and trivalent impurities, (Mg^{2+} , Zn^{2+} , Co^{2+} , Fe^{3+})-doped c-LN, employs structure A, whereas tetravalent impurities, (Zr^{4+} , Ti^{4+} , Ce^{4+})-doped c-LN, has structure B. The Nb_{Li} concentration increases with increasing tetravalent impurity concentration. In contrast, the Nb_{Li} concentration decreases with increasing divalent and trivalent impurities. It is the valence of an impurity that determines the location of impurities, whether they will be attracted to the Li site or the Nb site.

References

- [1] T. Volk and M. Wöhlecke, “Lithium Niobate Defects, Photorefraction and Ferroelectric Switching” (Springer, 2008).
- [2] C. Koyama, J. Nozawa, K. Maeda, K. Fujiwara, and S. Uda, J. Appl. Phys. **117**, 014102 (2015).
- [3] S. Uda, “Chapter 4; Stoichiometry of oxide crystals”, *Handbook of Crystal Growth, Vol. 1A: Fundamentals 2nd Ed.* (Elsevier, 2014), Edited by T. Nishinaga.

Keywords: oxide, doping, defects

Chihiro Koyama and Satoshi Uda (Crystal Chemistry Division)

E-mail: uda@imr.tohoku.ac.jp

URL: <http://www.uda-lab.imr.tohoku.ac.jp/index.html>

Heaviest Electron Detected by Quantum Oscillations

In heavy fermion physics, Yb compounds attract much interest because they are hole analogues to Ce compounds. Here, the heaviest electrons in YbCu₂Si₂ were detected by quantum oscillation measurements. It was found that valence fluctuations play a key role in the heavy electronic state, although YbCu₂Si₂ at ambient pressure is far from the magnetic quantum critical point.

The de Haas–van Alphen (dHvA) effect, which is the quantum oscillation in magnetization, is one of the most powerful experimental probes for detecting Fermi surfaces. The frequency is proportional to the cross-sectional area of the Fermi surface, and thus one can precisely determine the topology of the Fermi surface by rotating the field angle. Effective masses can also be obtained for each Fermi surface, meaning that the heavy electronic state can be directly observed microscopically.

dHvA experiments have been extensively done for Ce compounds, and the heavy electronic states have been established. The phenomena are basically understood in terms of the competition between the Kondo effect and the Ruderman–Kittel–Kasuya–Yosida (RKKY) interaction. The magnetic quantum critical point and the novel quantum phase, including the superconductivity, are the central issues in correlated electron systems. However, in Yb compounds, which are hole analogues to Ce compounds, Fermi surfaces with heavy electronic states are not very well understood experimentally because the dHvA experiments require a high-quality sample, a high field, and low temperatures.

In this study, we focused on the intermediate-valence-fluctuating compound YbCu₂Si₂, which has no magnetic order at ambient pressure. The electronic specific heat coefficient is 150 mJ/K² mol, indicating a heavy electronic state. However, the band calculation, which does not include the many-body effect, resulted in a value of only 15 mJ/K² mol. Thus, a heavy Fermi surface with a 10-times-larger effective mass was expected in the experiments.

We performed the dHvA experiments using a high-quality single crystal of YbCu₂Si₂ under extreme conditions at temperatures down to 30 mK and at high fields up to 15 T [1]. Figure 1 shows the dHvA oscillation and its fast Fourier transform (FFT) spectrum. The dHvA branches denoted as α , β , γ , and ε correspond to the main Fermi surfaces. Among them, branch β is the heavy Fermi surface, with 43 m_0 (m_0 : rest mass of electron), which

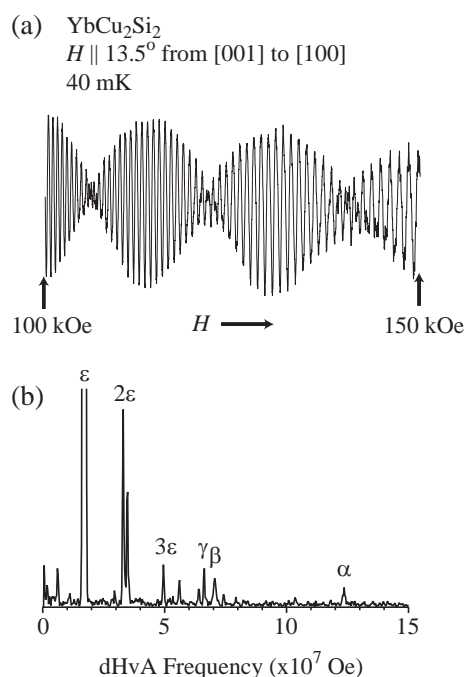


Fig. 1 Typical dHvA oscillation and its FFT spectrum in YbCu₂Si₂. Branch β has the heaviest cyclotron effective mass.

corresponds to the cylindrical Fermi surface centered at the X point in the Brillouin zone for a body-centered tetragonal structure. To our knowledge, the effective mass of 43 m_0 is the heaviest mass detected experimentally in dHvA studies of Yb compounds. Interestingly, the heavy mass in YbCu₂Si₂ is insensitive to the magnetic field. This is probably owing to the fact that YbCu₂Si₂ is a valence-fluctuating compound at ambient pressure, which is far from the magnetic quantum critical point ($P_c \approx 8$ GPa).

This work was done in collaboration with F. Honda, Y. Homma, D. X. Li, R. Settai, H. Harima, and Y. Onuki.

References

- [1] D. Aoki, F. Honda, Y. Homma, D. X. Li, R. Settai, H. Harima, and Y. Onuki, *J. Phys. Soc. Jpn.* **84**, 035002 (2015).

Keywords: Fermi surface, heavy fermion
 Dai Aoki (Actinide Materials Science Division)
 E-mail: aoki@imr.tohoku.ac.jp
 URL: <http://actinide.imr.tohoku.ac.jp/>

Effect of Ti Concentration on Chemically Ordered Regions in $\text{Pb}(\text{Mg}_{1/3}\text{Nb}_{2/3})\text{O}_3\text{-PbTiO}_3$ Epitaxial Thin Films

Although controversies still exist, the relaxor phenomenon in $\text{Pb}(\text{Mg}_{1/3}\text{Nb}_{2/3})\text{O}_3$ (PMN) is believed to arise from a heterogeneous structure consisting of a polar nano-region (PNR) and a chemically ordered region (COR). In the PNR, Mg and Nb are randomly arranged, thus giving rise to frustration, which is the origin of the phenomenon. In the COR, these elements are ordered, and thus they inhibit the fluctuation. In this study, we investigated the effects of Ti substitution on the stability of CORs.

We prepared $(1-x)\text{Pb}(\text{Mg}_{1/3}\text{Nb}_{2/3})\text{O}_3\text{-}x\text{PbTiO}_3$ (PMN- x PT) thin films by a chemical solution deposition process on SrTiO_3 (001) single-crystal substrates [1, 2]. The morphotropic phase boundary (MPB) was located at approximately $x = 0.6$. Our X-ray diffraction studies revealed that the deposited films were pseudocubic up to approximately $x = 0.5$, whereas tetragonality increased beyond this composition, suggesting a phase transformation [3]. This means that COR regions may exist below this value, and accordingly, we carried out structural examinations by using transmission electron microscopy (TEM).

The electron diffraction (ED) patterns from PMN- x PT specimens with $x = 0\text{--}0.5$ exhibited superlattice reflections at $1/2\ 1/2\ 1/2$ and other corresponding positions, indicating the formation of CORs. It was also noted that the intensities of the superlattice reflections decreased with increasing Ti content, x . However, the ED patterns only gave an average structure; real-space examination was needed.

Figures 1 (a), (b), and (c) show high-angle annular detector dark-field (HAADF) scanning transmission electron microscope (STEM) images of PMN- x PT films with $x = 0, 0.4$, and 0.5 , respectively. (Each set consists of wide-view images, magnified images, and diffractograms.) Because an HAADF-STEM image is basically that of Z-contrast, chemical ordering can be directly estimated by the intensity variations of the atomic images. The CORs thus obtained are indicated by solid rectangles in Fig. 1. As seen in the figure, each COR extends only up to 2 nm, or several unit cells, and they are distributed randomly within the film. It is also evident that an increase in Ti content led to the suppression of CORs. The driving force for the growth of CORs has its origin in the strain resulting from the difference of B-site cation radius, Mg^{2+} :0.072 nm and Nb^{5+} :0.067 nm, as well as in the electrical neutrality ($\text{Mg}^{2+}:\text{Nb}^{5+} = 1:2$). Overall, it can be said that CORs have intrinsic structural frustration and that Ti^{4+} mediates this situation.

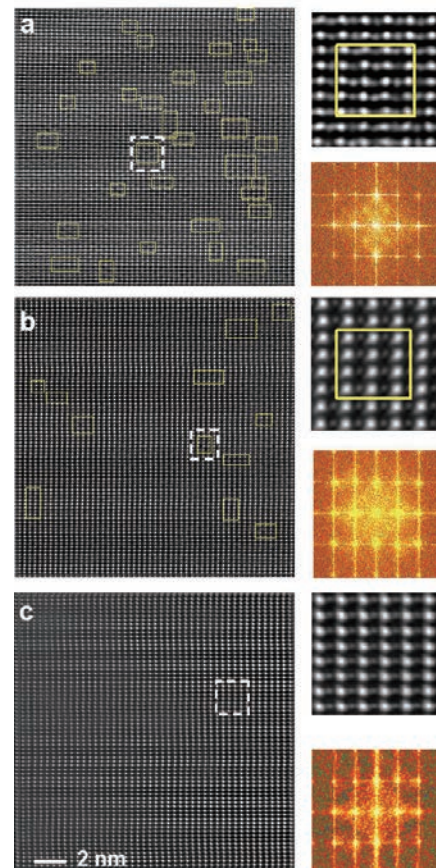


Fig. 1 Atomic-resolution HAADF-STEM images of (a) PMN, (b) PMN-0.4PT, (c) PMN-0.5PT. Diffractograms of the images and magnified images of a typical region marked with the white broken squares are also displayed. The solid lines in the HAADF-STEM images show CORs.

References

- [1] T. Kiguchi, Y. Misaka, M. Nishijima, N. Sakamoto, N. Wakiya, H. Suzuki, and T. J. Konno, *J. Ceram. Soc. Jpn.* **121**, 236 (2013).
- [2] Y. Misaka, T. Kiguchi, K. Sato, T. Nishimatsu, T. Yamada, N. Usami, and T. J. Konno, *Key Eng. Mater.* **582**, 19 (2014).
- [3] C. Fan, T. Kiguchi, A. Akama, and T. J. Konno, *J. Ceram. Soc. Jpn.* **123**, 565 (2015).

Keywords: dielectric properties, nanostructure, transmission electron microscopy (TEM)

Takanori Kiguchi (Materials Science of Non-Stoichiometric Compounds Division)

E-mail: tkiguchi@imr.tohoku.ac.jp

URL: <http://konno-lab.imr.tohoku.ac.jp/index.html>

Research Centers

IMR KINKEN Research Highlights 2016



Effects of Re Addition on Hydrogen Isotope Trapping in W Irradiated with High-energy Fe Ions at Elevated Temperatures

International Research Center for Nuclear Materials Science

Fusion power has been developed as an almost inexhaustible energy source for the future. Nuclear reactions of hydrogen isotopes, *i.e.*, deuterium (D) and tritium (T), are maintained in high-temperature plasma generated in a vacuum vessel lined with a refractory material such as tungsten (W). In this study, radiation-induced defects in W and trapping of D were successfully characterized by positron-annihilation spectroscopy (PAS).

Fusion power has been developed as an almost inexhaustible energy source for future generations. A large amount of energy (~keV) will be provided through controlled nuclear fusion reactions of D and T in high-temperature plasma, together with high energy He (3.5 MeV) and neutrons (14 MeV). The inner surfaces of reactor cores will be coated with refractory materials. Current designs of fusion reactors use W as a covering material because of its high melting point.

Tritium is a radioisotope of hydrogen, and hence the release of T from fusion power plants should be strictly controlled under both normal operating and accidental conditions. For this purpose, the amount of T in a vacuum vessel should be less than a certain amount. However, neutron irradiation of W induces defects, which then trap hydrogen isotopes, increasing T retention. The main objectives of this study were to understand the trapping of hydrogen isotopes in radiation-induced defects in W and to develop techniques to mitigate the radiation effects.

Neutron irradiation of W and W alloys in the research reactor BR2 has been performed through a collaboration program of the International Research Center for Nuclear Materials Science. Deuterium retention in these irradiated specimens will be examined by exposing the specimens to D plasma and D₂ gas after cooling of neutron-induced radioactivity.

Prior to the tests of neutron-irradiated specimens, the effects of Re addition were investigated using surrogate irradiation with 6.4 MeV Fe ions. Disks of W and a W-5Re alloy were irradiated with 6.4 MeV Fe ions at 523–1273 K up to 5 dpa (displacement per atom) at the Bragg peak. The specimens were exposed to D₂ gas at 673 K for 10 h. The microstructures of specimens were examined using positron-annihilation spectroscopy (PAS),

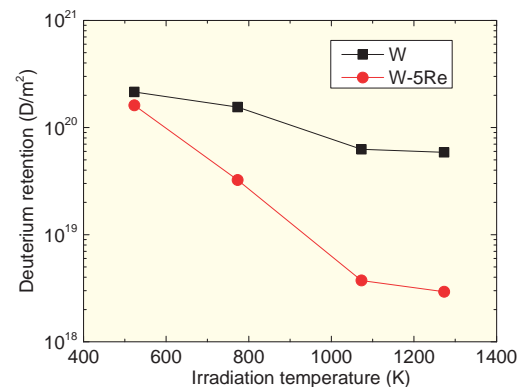


Fig. 1 D retention in W and W-5Re irradiated at various temperatures with 6.4 MeV Fe ions to the peak damage level of 0.5 dpa and then exposed to D₂ gas at a temperature of 673 K and a pressure of 100 kPa for 10 h.

whereas D retention was measured using nuclear reaction analysis (NRA).

The values of D retention in W and W-5Re are plotted against irradiation temperature in Fig. 1. The D retention in W-5Re was comparable to that in W after irradiation at 523 K. However, after irradiation at higher temperatures (>1073 K), the D retention in W-5Re was lower than that in W by one order of magnitude. PAS showed that this reduced D retention in W-5Re was due to faster recovery of vacancy-type defects (vacancies and vacancy clusters). These observations suggest that the addition of Re is effective in reducing trap-site density after irradiation of high-energy particles [1]. The effects of Re addition after neutron irradiation will be examined in the near future using the specimens irradiated in BR2.

References

- [1] Y. Hatano, K. Ami, V. Kh. Alimov, S. Kondo, T. Hinoki, T. Toyama, M. Fukuda, A. Hasegawa, K. Sugiyama, Y. Oya, M. Oyaidzu, and T. Hayashi, Nucl. Mater. Energ. (2016) in press.

Yuji Hatano (Corresponding Author, Hydrogen Isotope Research Center, Organization for Promotion of Research, University of Toyama)

E-mail: hatano@ctg.u-toyama.ac.jp

Yasuyoshi Nagai (Head of International Research Center for Nuclear Materials Science)

E-mail: nagai@imr.tohoku.ac.jp

URL: <http://www.imr-oarai.jp/index.html>

Single-crystal Growth and Magnetism of New Heavy-fermion Compound UPd₂Cd₂₀

International Research Center for Nuclear Materials Science

We succeeded in growing a high-quality single crystal of the new ternary uranium compound UPd₂Cd₂₀. From the electrical resistivity, magnetic properties, and specific heat experiments, UPd₂Cd₂₀ was found to be an antiferromagnetic heavy-fermion compound with a Néel temperature, T_N , of 5 K. It also exhibits a large electronic specific heat coefficient, γ , exceeding 700 mJ/(mol·K²).

Uranium (U) compounds have been intensively studied because of interesting phenomena such as the coexistence of superconductivity and magnetic and its heavy-fermion (HF) characteristics. The origin of these characteristic features in U compounds is responsible for 5f electrons in U atoms, which is an intermediate state between localized 4f and itinerant d electron systems.

Recently, a series of compounds with the formula UT₂X₂₀ (T: transition metal, X: Al, Zn), which crystallizes into a cubic CeCr₂Al₂₀-type structure [Fig. 1(a)] showed HF and metamagnetic behavior [1]. Substituting T and X metals, we can control the ground state, *i.e.*, the hybridization effect between the 5f and conduction electrons. To study the quantum critical point (QCP), we succeeded in growing a new isostructural compound of UPd₂Cd₂₀, with X = Cd, as shown in Fig. 1(b) [2].

X-ray diffraction experiments revealed that UPd₂Cd₂₀ crystallized into a CeCr₂Al₂₀-type structure without impurity phases and with a small residual resistivity, meaning that the obtained crystals are high quality. The drop in the magnetic susceptibility, χ , and the λ -shaped anomaly in the specific heat, C , in Fig. 2 indicate that UPd₂Cd₂₀ is an antiferromagnet (AF) with $T_N = 5$ K. UPd₂Cd₂₀ shows a broad maximum in χ at $T_{\chi\max}$ and a large electronic specific heat coefficient, γ , exceeding 700 mJ/(mol·K²). This value was estimated by extrapolating from C/T ($T \rightarrow 0$), which is a characteristic behavior in HF systems. The coexistence of AF and HF states implies that UPd₂Cd₂₀ is in the vicinity of QCP, and we succeeded in controlling the hybridization effect in the UT₂X₂₀ system.

To elucidate the AF and HF states in UPd₂Cd₂₀, further experimental measurements such as the de Haas–van Alphen effect and magnetization in high magnetic fields are in progress.

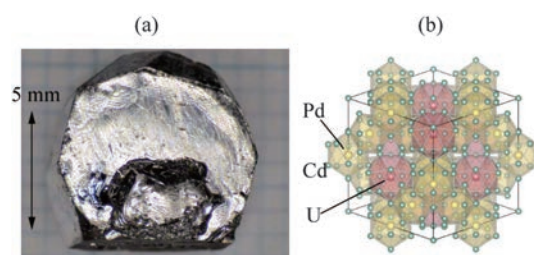


Fig. 1 (a) Crystal structure of UPd₂Cd₂₀. (b) Photograph of obtained crystal with a large size of 5 × 5 × 3 mm.

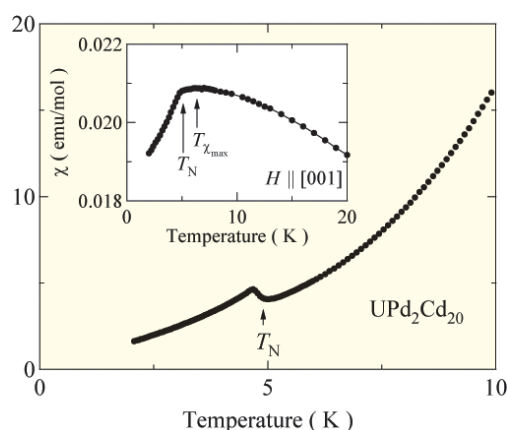


Fig. 2 Temperature dependence of the specific heat, C , indicating a magnetic transition at T_N . Inset shows the temperature dependence of magnetic susceptibility, indicating a broad maximum at $T_{\chi\max}$ and a rapid decrease at T_N .

References

- [1] Y. Hirose, T. Takeuchi, F. Honda, S. Yoshiuchi, M. Hagiwara, E. Yamamoto, Y. Haga, R. Settai, and Y. Ōnuki, *J. Phys. Soc. Jpn.* **84**, 074704 (2015).
- [2] H. Doto, Y. Hirose, F. Honda, D. Li, Y. Homma, D. Aoki, and R. Settai, *Physics Procedia* **75**, 56 (2015).

Yusuke Hirose (Corresponding Author, Department of Physics, Niigata University)

E-mail: yhirose@phys.sc.niigata-u.ac.jp

Yasuyoshi Nagai (Head of International Research Center for Nuclear Materials Science)

E-mail: nagai@imr.tohoku.ac.jp

URL: <http://www.imr-oarai.jp/index.html>

One-dimensional Hexagonal LiCoO₂ Crystals for Lithium Ion Battery Application

Cooperative Research and Development Center for Advanced Materials

One-dimensional LiCoO₂ crystals dominantly surrounding characteristic facets were synthesized by using a template-mediated flux growth method. The hexagonal cylindrical LiCoO₂ crystals were converted from the starting CoO whiskers. The results from single-particle measurements indicated excellent electrochemical performance.

Recently, much attention has been paid to lithium ion rechargeable batteries (LIBs) for use as power sources because of their high performance. LiCoO₂ is the most widely used cathode material in commercial LIBs owing to its good capacity retention, rate capability, and high structural reversibility.

The flux method, which is used for crystal growth from a liquid phase, is inexpensive, simple, and environmentally friendly. In the present study [1], one-dimensional (1D) LiCoO₂ crystals were grown by the template-mediated flux growth method. The precursor CoO (*Fm* $\bar{3}$ *m*, *a* = 0.4263 nm) whiskers were synthesized from LiCl and Co powder in a LiCl–KCl mixed flux. After lithiation to obtain CoO whiskers grown along the <111> direction, the obtained LiCoO₂ (*R* $\bar{3}$ *m*, *a* = 0.2819 and *c* = 1.4063 nm) crystals maintained the 1D morphology of the precursor CoO whiskers. The crystal shape was transformed from flat rectangular (CoO) to hexagonal cylindrical (LiCoO₂). In the cylindrical LiCoO₂ crystals, numerous hexagonal plated-shape crystals with sharp asymmetrical edges were stacked one dimensionally.

Figure 1 shows a TEM image of the 1D LiCoO₂ crystal and the corresponding selected area electron diffraction (SAED) patterns. Ordered diffraction reflections with no additional spots or diffuse streaks indicate that the 1D LiCoO₂ crystal had high crystallinity. Figure 2 shows schematics of atomic arrangements along the [211]CoO, [211]LiCoO₂, and [210 $\bar{1}$]LiCoO₂ directions. No significant changes in the arrangement of Co and O atoms occurred, even though the distance of the O–Co–O plane in CoO decreased somewhat owing to differences in the ionic radii of Co²⁺ in CoO and Co³⁺ in LiCoO₂.

The results from single-particle measurements, which were carried out in order to study the intrinsic electrochemical properties of the 1D LiCoO₂ crystal, indicated significantly better electrochemical responses than commercially available LiCoO₂.

The shape-controlled crystal growth will

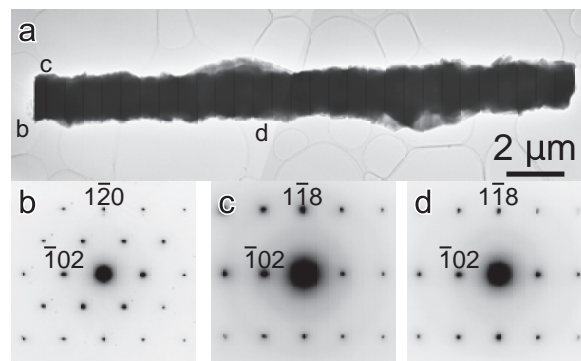


Fig. 1 (a) TEM image of 1D LiCoO₂ crystal and (b–d) corresponding SAED patterns.

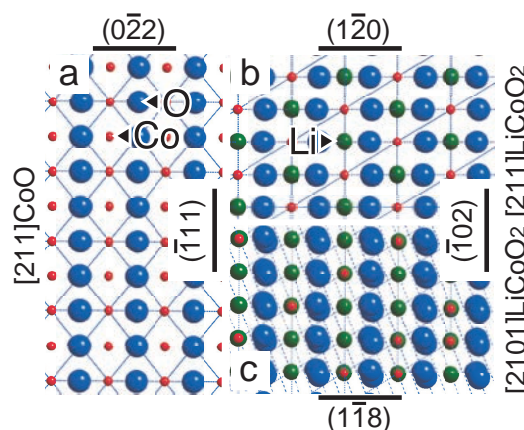


Fig. 2 Schematic of atomic arrangements along the (a) CoO [211] direction and the LiCoO₂ (b) [211] and (c) [210 $\bar{1}$] directions.

contribute to the further development of new advanced materials with a wide range of technological applications.

References

- [1] N. Zetsu, K. Nishikawa, K. Yubuta, K. Sakurai, Y. Yamamoto, Y. Mizuno, S. Oishi, and K. Teshima, *J. Mater. Chem. A* **3**, 17016 (2015).

Kunio Yubuta (Corresponding Author, Cooperative Research and Development Center for Advanced Materials)

E-mail: yubuta@imr.tohoku.ac.jp

Tadashi Furuhashi (Head of Cooperative Research and Development Center for Advanced Materials)

E-mail: crdam@imr.tohoku.ac.jp

URL: <http://www.crdam.imr.tohoku.ac.jp/index2.html>

Development of a 25 T Cryogen-free Superconducting Magnet

High Field Laboratory for Superconducting Materials

A 25 T cryogen-free superconducting magnet (25 T-CSM) was successfully developed. The 25 T-CSM consists of a 14 T low-temperature superconducting (LTS) outer coil and an 11 T high-temperature superconducting (HTS) inner coil. We succeeded in generating a 24.6 T field within a 1-h energizing time. We thus broke the record for the world's highest magnetic field in cryogen-free superconducting magnets.

Cryogen-free superconducting magnets (CSMs) are widely used nowadays because they can be operated without a cryogenic liquid. The maximum magnetic field generated by CSMs has increased year by year, as shown in the top image of Fig. 1, and most of these successes were obtained by the High Field Laboratory for Superconducting Materials (HFLSM). Recently, we achieved the world's highest magnetic field for CSMs of 24.6 T, denoted as 25 T-CSM. 25 T-CSM consists of an inner high-strength $\text{Bi}_2\text{Sr}_2\text{Ca}_2\text{Cu}_3\text{O}_y$ (Bi2223) coil, a middle high-strength CuNb/Nb₃Sn Rutherford cable coil, and an outer NbTi Rutherford cable coil (bottom image of Fig. 1) [1]. The outer two low-temperature superconducting (LTS) coils are connected in series and are operated by one power supply. The LTS coils, with a 300 mm bore, generate a 14 T field by an 851 A operating current. The Bi2223 insert coil generates 11 T without a background field and 10.6 T with a 14 T background field. The 24.6 T field is obtained in a 52 mm room-temperature bore within 1-h charging by a simultaneous energizing of the LTS and the HTS coils [2]. The HTS and LTS coils are separated thermally and cooled by two GM and two GM/JT cryocoolers, respectively.

The 25 T-CSM enables us a long time in-field heat treatment and a high sensitive experiment in low temperatures. A He-gas flow cryostat, a ³He refrigerator, and a ³He-⁴He dilution refrigerator will be available. The current-voltage measurements of superconducting wires with a noise level approximately one order of magnitude less than those of hybrid magnets were confirmed.

References

- [1] S. Awaji, K. Watanabe, H. Oguro, S. Hanai, H. Miyazaki, M. Takahashi, S. Ioka, M. Sugimoto, H. Tsubouchi, S. Fujita, M. Daibo, Y. Iijima, and H. Kumakura, *IEEE Trans. Appl. Supercond.* **24**, 4302005 (2014).
- [2] S. Awaji, H. Oguro, K. Watanabe, H. Miyazaki, S. Hanai, T.

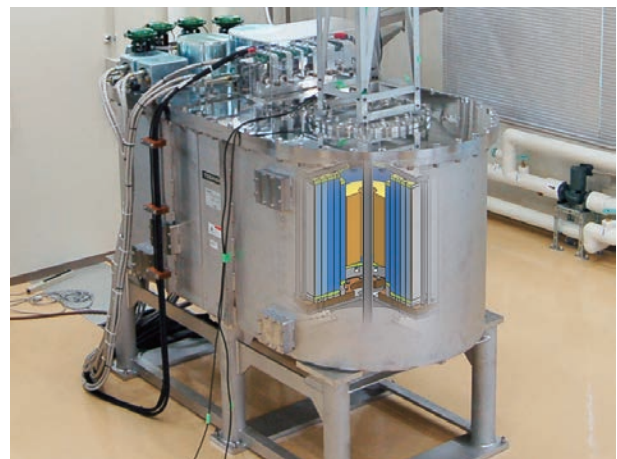
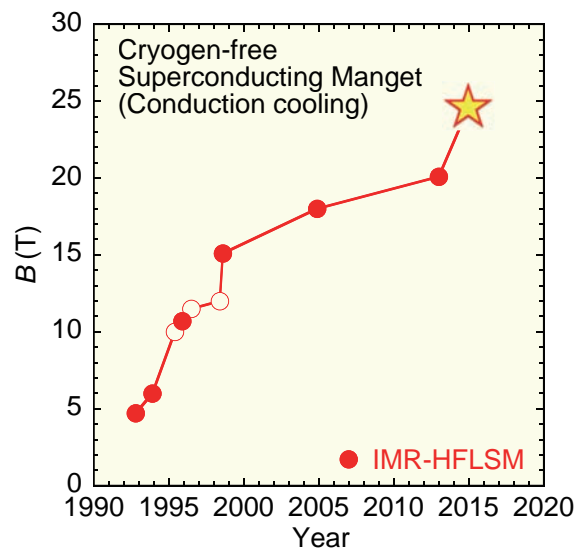


Fig. 1 (top) Progress of cryogen-free superconducting magnets (CSMs). 25 T-CSM has rewritten the world record of CSMs. (bottom) Photo of the 25 T-CSM in the HFLSM annex building.

Tosaka, and S. Ioka, *IEEE Trans. Appl. Supercond.* to be submitted.

Satoshi Awaji and Kazuo Watanabe (Corresponding Authors, High Field Laboratory for Superconducting Materials)

E-mail: awaji@imr.tohoku.ac.jp

Hiroyuki Nojiri (Head of High Field Laboratory for Superconducting Materials)

E-mail: nojiri@imr.tohoku.ac.jp

URL: <http://www.hflsm.imr.tohoku.ac.jp/>

Scientific Breakthrough toward Creation of New Industrial Materials

Kansai Center for Industrial Materials Research

Institute for Materials Research (IMR) has launched the Kansai Center, a comprehensive institute-wide effort that pairs IMR's research groups across the innovation spectrum to solve today's industrial challenges and transform tomorrow's global energy problems. The center was established in April 2011 based on an agreement between IMR, Osaka Prefecture Government, and enterprises in the Kansai area sponsored by the government, taking over Osaka Center project.

The Kansai Center was established in Osaka as a special unit in the Institute for Materials Research (IMR), Tohoku University, in April 2011 based on an agreement with Osaka Prefecture Government. The Center is sponsored by the government (Ministry of Education, Culture, Sports, Science and Technology) and it took over the Osaka Center, which carried out its mission from 2006 to 2011. The Kansai Center has three missions: first, to solve technical problems that industries have struggled to resolve; second, to provide academic output to industries, with the aim of applying such output to society; and third, to help educate next-generation materials scientists and researchers in universities and enterprises. We have organized a bimonthly forum named "Monodukuri Kisokoza," which focuses on special topics regarding materials and processing. Projects are conducted through wide collaborations between the government, universities, research institutions, and other organizations. The Center has four venues to cover the Kansai area: the Osaka office at Osaka Prefecture University, the Hyogo office at University of Hyogo, the Sendai office in IMR, and Monodzukuri Business Information Center Osaka (MOBIO) in the Creation Core Higashi-Osaka, a governmental body where sixteen local universities and one college are located to facilitate collaboration with various industries.

The Center has developed various materials and processes in collaboration with industry, universities, and government organizations. One of them is a bioactive surface of implant TiNbSn alloy, which has been developed by IMR. Anodic oxidation (AO) and subsequent hot-water (HW) treatment enhanced apatite formation after immersing the alloy in Hank's solution (Fig. 1). A high bonding strength between the TiNbSn alloy and rabbit femurs was obtained as compared to untreated TiNbSn from pull-out mechanical tests in animal experiments [Fig. 2(a)] [1]. Cross-sectional EDX analysis for the implanted TiNbSn alloy in rabbits over six weeks revealed incorporation of Ca and P in the TiO₂ layer from bone, suggesting diffusion of constituent elements of

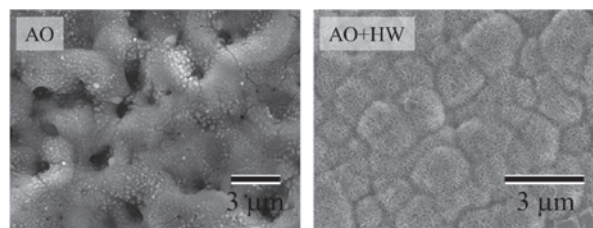


Fig. 1 SEM images of untreated and AO+HW treated TiNbSn and CP-Ti discs.

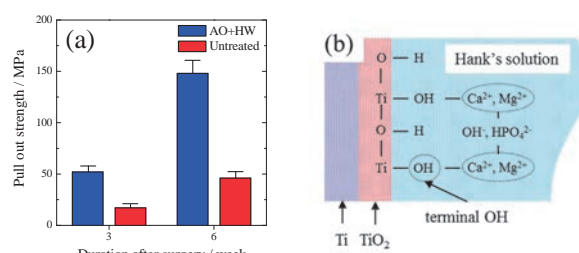


Fig. 2 (a) Failure load 3 and 6 weeks after implantation and (b) schematic illustration of apatite formation after immersion in Hank's solution.

animal bone to TiO₂, which is responsible for the high bonding strength. Hot-water treatment for the anodized TiNbSn promoted apatite formation owing to the hydrophilic surface of TiO₂ [Fig. 2(b)]. Strong bonding was attributed to the inter-diffusion of Ca and P between TiO₂ and animal bone. It is concluded that bioactive properties were imparted to the TiNbSn alloy coated by anodic oxidation of TiO₂.

Similar collaboration studies for practical applications utilizing academic knowledge and industrial technology have been in progress. The Kansai Center will make an effort to innovate in the metallic materials industry through an alliance with partners in the Kansai area and will promote scientific research of materials science.

References

- [1] H. Tanaka, Y. Mori, A. Noro, A. Kogure, M. Kamimura, N. Yamada, S. Hanada, N. Masahashi, and E. Itoi, Plos. (2016) accepted.

Naoya Masahashi (Head of Kansai Center for Industrial Materials Research)

E-mail: masahasi@imr.tohoku.ac.jp

URL: <http://www.kansaicenter.imr.tohoku.ac.jp>

※Kansai Center has been reorganized in Trans-Regional Corporation Center for Industrial Materials Research since 2016.

Supercomputing to Understand Materials Processing and Materials Properties

Center for Computational Materials Science

The Center for Computational Materials Science supports multiscale supercomputing in materials science. Herein, we introduce two major activities selected from approximately 120 users. Dr. Deb Nath analyzes solidification behavior, which is of fundamental importance in manufacturing process, and Dr. Wakeda and Prof. Ogata predict critical resolved shear stress, a typical mechanical property of alloys.

Interfacial free energy and the stiffness of Cu–Al alloys obtained by atomistic simulations^{a)}

Applying classical nucleation theory to a spherical crystal embedded in an undercooled melt, one obtains the interfacial free energy as a function of crystal radius, r [1], $\sigma_{sl} = (0.5 \cdot \Delta T \cdot \Delta H \cdot r) / T_M$ (1), where T_M is the melting point and ΔH is the change of enthalpy. Liquid Cu₅₀Al₅₀ alloys are obtained by heating a mixture of Cu and Al at a constant temperature. Then, different sizes of solid Cu₅₀Al₅₀ spheres are inserted into the liquid Cu₅₀Al₅₀. The whole system is relaxed for several time steps and then heated isothermally in order to understand the critical temperature for each solid Cu₅₀Al₅₀ sphere. Varying the size of the solid Cu₅₀Al₅₀ sphere in the same Cu₅₀Al₅₀ liquid cell, the undercooling temperature versus the inverse of the critical radius of the solid Cu₅₀Al₅₀ sphere is plotted in Fig. 1. The anisotropy of the interfacial free energy and its stiffness will be determined by the capillary fluctuation method [2].

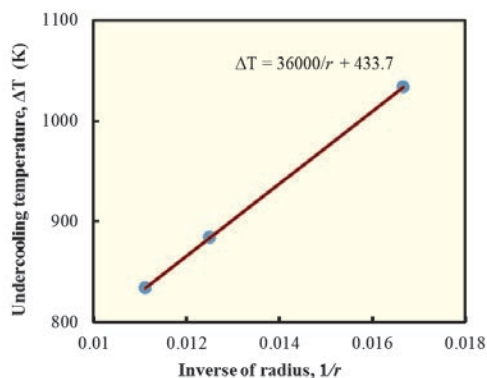


Fig. 1 Undercooling temperature as a function of $1/r$ to obtain the interfacial free energy of the solid–liquid interface of Cu₅₀Al₅₀.

References

- [1] Y. Watanabe, Y. Shibuta, and T. Suzuki, *ISIJ international* **50**, 1158 (2010).
 [2] J.J. Hoyt, M. Asta and A. Karma, *Phys. Rev. Lett.* **86**, 5530 (2001).

A priori theoretical prediction of solute strengthening of iron alloy^{b)}

An a priori theoretical prediction of the solute strengthening of a metal is required for high throughput screening of alloys in structural materials design. Because plastic deformation in a metal is mainly caused by dislocations, the interaction between dislocations and solute atoms is a crucial factor for controlling the strength of metals. Here, we focused on iron alloys and constructed the prediction framework for strengthening by solute atoms based on atomistic theory. In the case of bcc iron, the critical resolved shear stress CRSS (stress at onset of plastic deformation) is dominated by screw dislocation motion, which is discretized into kink nucleation and kink migration processes. We evaluated the energy barrier for the two processes under the effect of solute atoms using an atomistic model based on semi-empirical interatomic potentials [3] and calculated the dislocation velocity by following the thermal activation theory. The CRSS can be predicted by the dislocation velocity at arbitrary temperatures, solute concentrations, and strain rates [4].

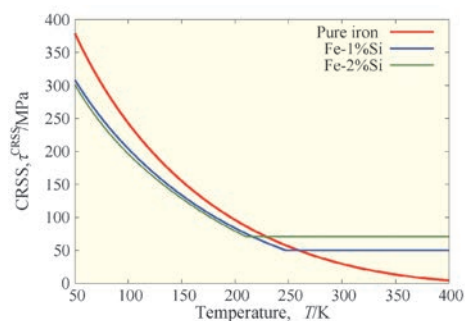


Fig. 2 The predicted CRSS of pure Fe and Fe–Si alloys [4].

- [3] M. Wakeda, H. Kimizuka, and S. Ogata, *J. Japan Inst. Met. Mater.* **77**, 409 (2013).
 [4] S. Shinzato, M. Wakeda, and S. Ogata, *J. Japan Inst. Met. Mater.* **80**, 197 (2016).

a) Sankar Kumar Deb Nath [Corresponding Author, Computational Materials Research Initiative (CMRI)]

E-mail: debnath@imr.tohoku.ac.jp

b) Masato Wakeda¹ and Shigenobu Ogata^{1, 2} (Corresponding Authors, ¹Graduate School of Engineering Science, Osaka U., ²Center for elements strategy initiative for structural materials, Kyoto U.)

E-mail: wakeda@me.es.osaka-u.ac.jp

Tetsuo Mohri (Head of Center for Computational Materials Science)

URL: <http://www-lab.imr.tohoku.ac.jp/~ccms/Eng/index.php>

Atomic-level Description of Cutting-Edge Energy Materials for a Sustainable Society

Collaborative Research Center on Energy Materials

In order to attain clean and economical energy systems, the Center creates and studies advanced energy materials with superior functional properties that have important roles in energy generation and consumption. Through joint efforts in both science and engineering, high-performance energy materials that efficiently convert and transport energy are investigated.

At our Center, research and development focus on the atomic-level control of the multiple structure–property relationships of advanced energy materials, as well as on the design of devices that lead to effective carrier conversion, high-speed energy transport, and increasing renewable energy production. This can be achieved by integrated control of spin, electron, ion, hole, and phonon-like carriers.

One of the Center's research activities is directed towards the development of materials that can be used in sustainable gas storage/separation technologies. This requires precise control of the structure on an atomic level and accurate analysis of the interactions that occur during the adsorption process.

In the Material Processing and Social Implementation Division, we estimate the important properties of various nanoporous materials using highly accurate computational methods in order to accelerate the experimental realization of novel storage media. In the search for novel functional adsorbents, metal–organic framework (MOF) materials with unprecedented regular nano-sized spaces have been studied.

Recently, a new soft porous coordination polymer, Cu^{2+} (5-azidoisophthalate), with adaptable pores that selectively adsorb CO from a CO/N₂ gas mixture was discovered. The key feature of this structure is the presence of two channels having different pore sizes, with the size of the small one increasing owing to the interaction of CO molecules with the Cu^{2+} sites, as shown in Fig. 1a. This allows one to control the next step of the separation process. In agreement with the experimental data, the calculation results showed a remarkable distinction in adsorption properties of the CO-coordinated MOF towards CO and N₂ separation. The electron distribution of the CO adsorption process indicated favorable attraction between the guest molecule and the small channel of the host structure. In the case of N₂, the electron distribution showed repulsion between nitrogen molecules and the host framework. Thus, high selectivity is achieved by the synergetic effect of the local interaction between CO and accessible Cu^{2+} metal sites and a

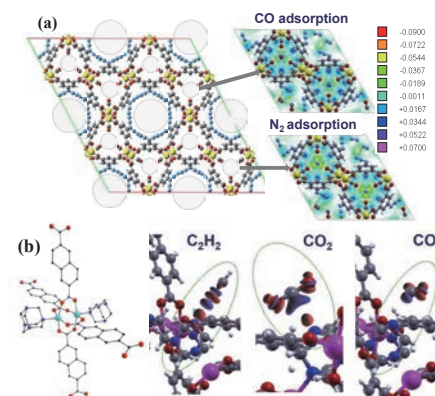


Fig. 1 (a) Cu^{2+} (5-azidoisophthalate) structure and electron density contours of CO and N₂ adsorbed inside small channels. (b) Fragment of $\text{Zn}_4(\text{dmf})(\text{ndc})_4(\text{ur})_2$ with urotropine ligand and charge density isosurfaces for the C_2H_2 , CO_2 , and CO interactions.

global transformation of the framework [1].

The adsorption properties of the porous $\text{Zn}_4(\text{dmf})(\text{ndc})_4(\text{ur})_2$ structure were also investigated (see Fig. 1b). This material is a rare example of a microporous compound with open basic sites decorating the inner surface of the MOF host. It was found that the inclusion of the urotropine ligand into the MOF framework enhanced the adsorption of acetylene and carbon dioxide. Thus, only in the case of the C_2H_2 molecule, the most favorable attraction with the host is through the formation of a C–H \cdots N hydrogen bond between the H atoms of acetylene and the N atoms of urotropine [2]. The use of urotropine as a co-bridging ligand in metal–carboxylate MOFs may therefore result in a variety of other porous materials with notable basic functionality derived from non-coordinated N-centers.

References

- [1] H. Sato, W. Kosaka, R. Matsuda, A. Hori, Y. Hijikata, R. V. Belosludov, S. Sasaki, M. Takata, and S. Kitagawa, *Science* **343**, 167 (2014).
- [2] S. A. Sapchenko, D. N. Dybtsev, D. G. Samsonenko, R. V. Belosludov, V. R. Belosludov, Y. Kawazoe, M. Schroder, and V. M. Fedin, *Chem. Comm.* **51**, 13918 (2015).

Rodion Belosludov (Corresponding Author, Collaborative Research Center on Energy Materials)

E-mail: rodion@imr.tohoku.ac.jp

Shin-ichi Orimo (Head of Collaborative Research Center on Energy Materials)

E-mail: orimo@imr.tohoku.ac.jp

URL: <http://www.e-imr.imr.tohoku.ac.jp/>

Magnetization Reversal in Perpendicularly Magnetized FePt Dot and Antidot Arrays

International Collaboration Center (ICC-IMR)

FePt dot and antidot lattices with diameters 40 nm, 100 nm, and 200 nm were microfabricated by electron beam lithography. Magnetization reversal in these FePt nanoarrays was studied by magneto-optical Kerr effect and magnetic force microscopy. The FePt dots exhibited superferromagnetic behavior despite their complete isolation. Magnetic domain imaging revealed that the reversal processes showed a domain wall trap in the antidote lattices.

L_{10} -FePt alloy is one of the most promising materials for future ultrahigh density magnetic storage devices because of its huge uniaxial magnetocrystalline anisotropy ($K_u = 7 \times 10^7$ erg/cm³), which leads to a high thermal stability of magnetization at the nanometer scale. The aim of this international collaboration is to understand the magnetization reversal processes in FePt thin films, dots, and antidots. By using magneto-optic Kerr microscopy, we first studied the magnetization reversal in FePt thin films deposited on MgO (110) substrates exhibiting in-plane uniaxial magnetic anisotropy. The domain structure and magnetization reversal process strongly depended on the film thickness and the deposition temperature [1].

The magnetization reversal behavior for perpendicularly magnetized L_{10} -FePt (001) nanodots with different interdot spaces was also investigated by magnetic force microscopy (MFM). The dots, which were fully isolated, experienced only dipolar interaction; however, the array with the isolated FePt dots exhibited domain like features resembling the behaviour of percolated dots, indicating superferromagnetism in the FePt nanodot array [2].

We also studied the magnetic properties of a “negative” magnetic structure fabricated by lithography to create a mesh of “holes” in a continuous FePt magnetic thin film. These negative structures are called “antidots”, and the array of such antidots is called “magnetic antidot lattice (MAL)”. MALs are attracting much interest from the research community because of their potential lack of superparamagnetic limit to the bit size (in comparison to dot arrays). The major question is how a magnetic domain wall (DW) will behave in an MAL system with periodic defects. We fabricated MALs of perpendicularly magnetized FePt with the dimensions of the antidots ranging from 200 nm to 40 nm. MAL arrays with various types of lattices, such as square and honeycomb were

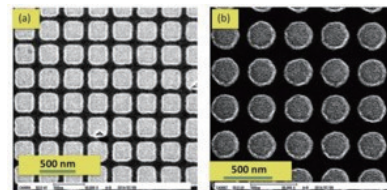


Fig. 1 SEM images of FePt antidot lattices with (a) rectangular and (b) circular holes.

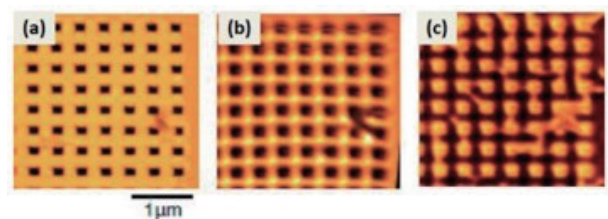


Fig. 2 (a) Morphology of a FePt antidot lattice with the dimension of 200 nm. The image shown in (b) is the magnetic domain structure taken post-remnant after positive saturation. (c) Magnetic domain imaged near a coercive field of $\mu_0H = -0.15$ T.

fabricated to study the effect of the lattice pattern on the magnetization reversal. Scanning electron microscopy (SEM) indicated that the size and shape of the antidot lattices were well controlled. Figure 1 shows the SEM images of two representative FePt MALs on MgO (100) substrates. Figure 2 shows the MFM images of an antidot lattice where the length of the antidots is 200 nm. It can be observed that the DWs are trapped between the antidot structures. Under external magnetic field, the domains show limited expansion within the antidot structures.

References

- [1] S. Mallick, S. Bedanta, T. Seki, and K. Takahashi, *J. Appl. Phys.* **116**, 133904 (2014).
- [2] S. Bedanta, T. Seki, H. Iwama, T. Shima, and K. Takahashi, *Appl. Phys. Lett.* **107**, 152410 (2015).

Subhankar Bedanta [Corresponding Author, National Institute of Science Education and Research (NISER), India]

E-mail: sbedanta@niser.ac.in

Gerrit Ernst-Wilhelm Bauer (Head of International Collaboration Center)

E-mail: icc-imr@imr.tohoku.ac.jp

URL: <http://www.icc-imr.imr.tohoku.ac.jp/>

Materials Science Advanced by Neutron Platform

Center of Neutron Science for Advanced Materials

The Center of Neutron Science for Advanced Materials is a unique neutron facility that has the background of novel material science in IMR. This center is constructing a state-of-the-art polarized neutron spectrometer, POLANO, at the Japan Proton Accelerator Research Complex (J-PARC/MLF.) To promote neutron science, we held a workshop and a J-PARC/MLF tour under collaboration with quantum-beam scientists at Tohoku University.

The Center of Neutron Science for Advanced Materials (CN-IMR) was established in 2010 with the aim of promoting novel materials science by using neutrons. The CN-IMR is constructing a new polarized neutron spectrometer, POLANO, at the Japan Proton Accelerator Research Complex (J-PARC/MLF) [1] as part of a joint project with the High Energy Accelerator Research Organization (KEK). The spectrometer will give a unique opportunity to measure the microscopic state in materials with separating pure magnetic correlations and atomic correlations. The first neutron beam will be received in 2016FY. The spectrometer will then be available for the collaborative research program of IMR.

In order to discuss novel science brought about through new materials and spectroscopic measurements, we held a two-day workshop entitled “Materials Science Advanced by Quantum-Beam Platform,” and more than twenty neutron scientists were invited to attend. Information on state-of-the-art techniques was exchanged among the participants and future studies utilizing polarized neutrons at POLANO were discussed.



Fig. 1 A photo of workshop held in IMR. More than forty neutron scientists were participated.



Fig. 2 A group photo of J-PARC/MLF tour.

Furthermore, a J-PARC/MLF tour was held for students and young researchers to provide an opportunity to visit the large facility and to learn the fundamentals as well as hear about the latest research in quantum-beam science. Sixteen students from four laboratories attended the tour. The lectures on neutron scattering and muon spin rotation techniques were given by four staff members from Tohoku University and KEK, which covered the historical aspects of quantum-beam science at Tohoku University. Students visited POLANO and saw the status of the construction. The tour was well received by the participants.

References

- [1] T. Yokoo, K. Ohoyama, S. Itoh, K. Iwasa, N. Kaneko, J. Suzuki, M. Ohkawara, K. Aizawa, S. Tasaki, T. Ino, K. Taketani, S. Ishimoto, M. Takeda, T. Oku, H. Kira, K. Hayashi, H. Kimura, and T. J. Sato, EPJ Web of Conferences **83**, 03018 (2015).

Masaki Fujita (Head of Center of Neutron Science for Advanced Materials)

E-mail: nc-imr@imr.tohoku.ac.jp

URL: <http://nc-imr.imr.tohoku.ac.jp/>

Artificially Produced Rare-Earth-Free Cosmic Magnet

Research and Development Center for Ultra High Efficiency
Nano-Crystalline Soft Magnetic Material

A hard magnetic $L1_0$ -FeNi phase with a chemical order parameter of 0.8 or higher, which is a higher grade than that found in cosmic meteorites, was produced artificially by utilizing an alloy design that shortens the formation time from hundreds of millions of years for natural meteorites to less than 300 h.

The present completely rare-earth-free magnet (Fe-Ni-metalloid alloy) with a chemical order parameter (S) of 0.8 or higher, as shown in Fig. 1 [1], was produced from NANOMET[®] [2] by partially replacing Fe with Ni. It was produced using the same production process as NANOMET[®]. Surprisingly, the addition of Ni, with a characteristic of soft magnetism by nature to NANOMET[®], changes from a soft magnetic alloy to a hard one (Fig. 2). This change is due to the artificial production of a highly ordered $L1_0$ -FeNi phase in the samples, where the phase is the same as that found in natural meteorites. Crystallization of the amorphous alloy drastically shortened the production time to 300 h from a couple of billion years for natural meteorites. Opposing characteristics, such as “extremely rapid quenching (non-equilibrium) and extremely slow cooling (extreme equilibrium)” and “soft and hard

magnetism” have been linked through serendipity.

The present results open a door for the development of completely rare-earth-free magnets with $S \geq 0.8$ for the first time. Going forward, we will come to understand fundamental magnetic properties before moving on to research and development of materials applications. Subsequently, we will select industrial problems and establish their solutions. Finally, we are planning to carry out studies using the magnet in demonstration motors as soon as possible.

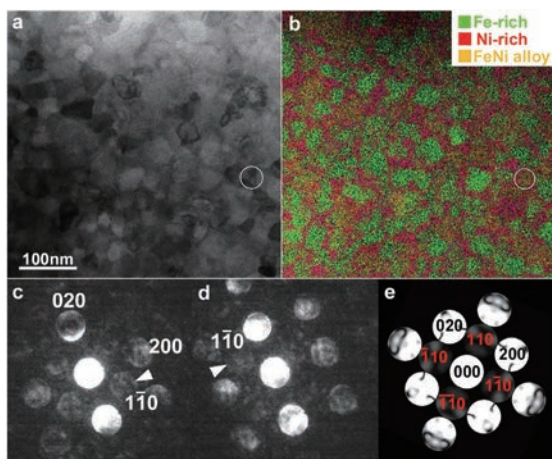


Fig. 1 (a) STEM bright-field image and (b) STEM-EDX elemental mapping. (c, d) Nanobeam electron diffraction taken from the area marked with circles in Figs. 1 (a, b). (e) Simulated NBD pattern of the $L1_0$ FeNi structure, with $S = 0.8$. Here, STEM and EDX stand for Scanning Transmission Electron Microscope and Energy Dispersive X-ray spectrometry, respectively.

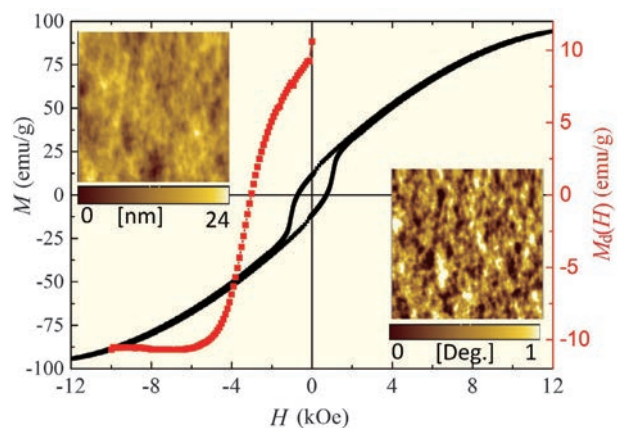


Fig. 2 Magnetic hysteresis (left: black) and dc demagnetization curves (right: red). Measurement conditions include applying a maximum magnetic field of ~ 12 kOe perpendicular to the ribbon plane for the M vs H curve and 10 kOe for the $M_d(H)$ vs H curve. Top inset shows the topographic AFM (Atomic Force Microscope) image, whereas the bottom inset is the corresponding magnetic force microscopy (MFM) image demonstrating the magnetic domains.

References

- [1] A. Makino, P. Sharma, K. Sato, A. Takeuchi, Y. Zhang, and K. Takenaka, *Sci. Rep.* **5**, 16627 (2015).
- [2] A. Makino, T. Kubota, C. Chang, M. Makabe, and A. Inoue, *J. Mag. Mag. Mater.* **320**, 2499 (2008).

Akira Takeuchi (Corresponding Author, Research and Development Center for Ultra High Efficiency Nano-Crystalline Soft Magnetic Material)
E-mail: takeuchi@imr.tohoku.ac.jp

Akihiro Makino (Head of Research and Development Center for Ultra High Efficiency Nano-Crystalline Soft Magnetic Material)
E-mail: nanoc@imr.tohoku.ac.jp

URL: <http://nanoc.imr.tohoku.ac.jp/eng/index.html>

Metallic Ground State in an Atomically Thin Superconductor Induced by an Electric Field

Laboratory of Low-Temperature Materials Science

Electric double-layer transistors composed of an interface between a crystalline solid and an ionic liquid provide a good opportunity to investigate the intrinsic nature of two-dimensional superconductors. Here, we report that an ion-gated ZrNCl superconducting surface with an effective thickness of approximately 1.8 nm reveals a metallic ground state with finite resistance, even in a weak magnetic field.

Recently emerging two-dimensional (2D) superconductors in atomically thin layers at heterogeneous interfaces are attracting growing interest in condensed matter physics. These systems are highly crystalline with lower normal-state electric resistance. They may therefore show the intrinsic nature of 2D superconductors, which is hidden by the disorder in conventional metallic thin films. An electric double-layer transistor (EDLT), which is composed of an interface between a crystalline solid and an ionic liquid, may be able to provide such a clean system because the conduction carriers are induced electrostatically at the atomically flat surfaces without introducing extrinsic disorder. Here, we report the transport properties of a ZrNCl EDLT under a magnetic field, H [1].

ZrNCl is known as an atomic-layer material with insulating behavior. In this study, we succeeded in converting its topmost surface into a superconductor with a transition temperature, T_c , of 14.5 K and an effective thickness of approximately 1.8 nm, which is less than its one-unit-cell thickness, by gating in the EDLT configuration, as shown in Fig. 1(a). Figure 1(b) shows the temperature dependence of the sheet resistance, $R_{\text{sheet}}(T)$, at a gate voltage, V_G , of 6.5 V in magnetic fields perpendicular to the conducting plane. In this Arrhenius plot, $R_{\text{sheet}}(T)$ exhibits activated behavior just below T_c (dashed lines), which can be well described by the conventional thermal creep phenomenon of quantum vortices. We found that at low temperatures, on the other hand, each $R_{\text{sheet}}(T)$ curve clearly deviates from the activated behavior and then crosses over to temperature-independent behavior down to the lowest temperature, even at $H = 0.05$ T, which is much lower than the upper critical field of approximately 2 T. The results imply that a metallic ground state exists in the wide region of a mixed state. This can be attributed to the intrinsic vortex

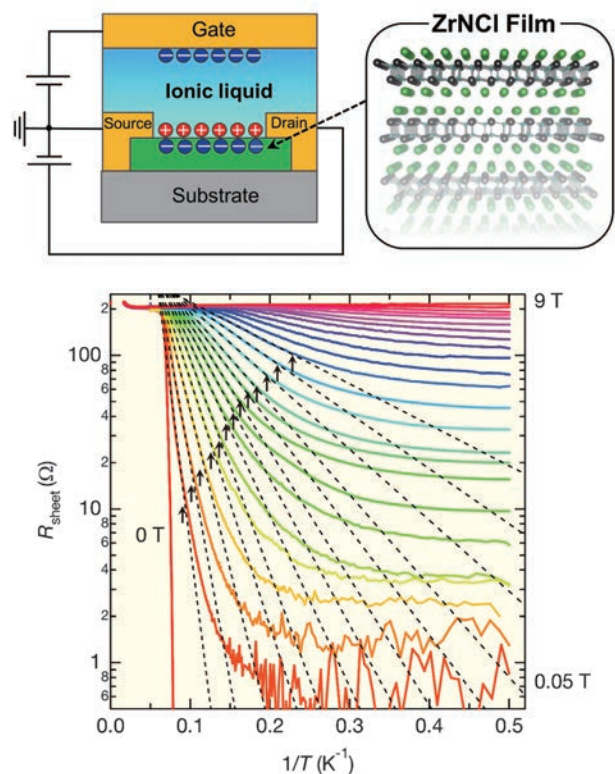


Fig. 1 (a) Schematic of EDLT. (b) Arrhenius plot of the sheet resistance of a ZrNCl EDLT at $V_G = 6.5$ V for different magnetic fields perpendicular to the surface.

creep motion driven by quantum mechanical processes, which has been difficult to observe in disordered metallic thin-film superconductors, resulting in either a superconducting or an insulating ground state.

Our results indicate that the EDLT provides a model platform of clean 2D superconductors with weak pinning and disorder.

References

- [1] Y. Saito, Y. Kasahara, J. Ye, Y. Iwasa, and T. Nojima, *Science* **350**, 409 (2015).

Tsutomu Nojima (Corresponding Author, Laboratory of Low-Temperature Materials Science)

E-mail: nojima@imr.tohoku.ac.jp

Takahiko Sasaki (Head of Laboratory of Low-Temperature Materials Science)

E-mail: ltcenter@imr.tohoku.ac.jp

URL: <http://ltsd.imr.tohoku.ac.jp/>

Research Facility for Physics and Chemistry of Radioactive and Nuclear Materials

Laboratory of Alpha-Ray Emitters

More than 170 species of radioisotopes and nuclear materials are available for study at the Laboratory of Alpha-ray Emitters. This laboratory is one of the most important centers around the world for studying the physical and chemical properties of radioactive materials such as actinide compounds. Researchers from many of the leading universities and institutes all over the country visit this facility every year to prepare a variety of materials and carry out chemical and physical measurements.

This laboratory has provided a research environment for the study of 170 radionuclides (RIs) and elements, especially alpha-ray emitters such as actinide elements, since 1960. The laboratory, originally located in the basement of the old Main Building 1, was moved to its present location in 1978. The lab's inventory of RIs, including actinide elements, is one of the largest among Japanese universities. The lab functions as an important source for the preparation of pure crystals of actinide compounds, providing them to other universities and to SORs.

The controlled area of this laboratory consists of three chemistry labs, three physical labs, a room for radioactivity measurements, a contamination test room, and storage rooms for RIs and nuclear materials. Each chemistry lab is equipped with local exhaust ventilation systems, which enables handling of unsealed radioactive materials. Gamma-ray spectrometers, a liquid scintillation counter, and an alpha-ray spectrometer are available in the radioactivity measurement room.

Correlated electron phenomena in actinide intermetallic compounds have attracted attentions. The formation of a heavy fermion state, where the effective mass of the conduction carriers become extremely large as a result of Kondo-type interactions between magnetic moments derived from the $5f$ state in actinides and conduction bands, is one of the central topics being studied because the high densities-of-state often lead to novel phase transitions, such as unconventional superconductivity.

The uranium compound URu_2Si_2 is one of those compounds. It is known as an unconventional superconductor coexisting with an unidentified electronically ordered state, called a "hidden order" [1].

It is therefore interesting to investigate the modification of the conduction electron behavior upon introduction of $5f$ electrons in a metal. This can be accomplished by detecting changes in the Fermi surface formed by conduction electrons via the de Haas-van Alphen technique. In fact, it has recently been demonstrated in a cerium-based system, $CeRu_2Si_2$, with the same crystal structure, where the

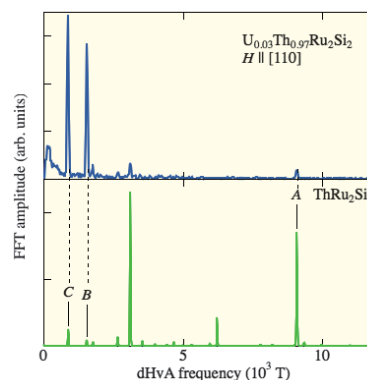


Fig. 1 Fourier transforms of de Haas-van Alphen oscillations in pure $ThRu_2Si_2$ and in uranium-substituted $ThRu_2Si_2$. The frequencies are proportional to the cross sectional areas of the Fermi surfaces.

magnetic moment of the $4f$ electron in cerium is gradually incorporated into the Fermi surfaces, leading to their volume change, which is interpreted in terms of Kondo interaction [2].

In the case of URu_2Si_2 , however, the situation looks quite different. Recent attempts to introduce uranium into the host metal $ThRu_2Si_2$ only resulted in a change in the effective mass of the conduction electrons without changing the volume. A typical experimental result is shown in Fig. 1, where the cross sectional areas are shown both for pure $ThRu_2Si_2$ and the dilute alloy $(U_{0.03}Th_{0.97})Ru_2Si_2$ [3]. The enhancement of the conduction carriers is also reflected in the bulk properties, such as specific heat [3, 4]. The significantly different behavior of the actinide system as compared to the well-known cerium system might reflect novel characteristics of $5f$ wave functions in actinides.

References

- [1] J.A. Mydosh and P.M. Oppeneer, *Rev. Mod. Phys.* **83**, 1301 (2011).
- [2] H. Aoki, N. Kimura, and T. Terashima, *J. Phys. Soc. Jpn.* **83**, 072001 (2014).
- [3] Y. Haga, Y. Matsumoto, N. Tateiwa, E. Yamamoto, N. Kimura, T. Yamamura, and Z. Fisk, *J. Phys.: Conf. Ser.* **592**, 012036 (2015).
- [4] H. Amitsuka and T. Sakakibara, *J. Phys. Soc. Jpn.* **63**, 736 (1994).

Tomoo Yamamura (Head of Laboratory of Alpha-Ray Emitters)

E-mail: yamamura@imr.tohoku.ac.jp

URL: <http://alpha.imr.tohoku.ac.jp/>

Improved Analytical Procedures for Highly Sensitive and Precise Determination of Trace Elements in Metallic Materials

Analytical Research Core for Advanced Materials

In routine elemental analysis, the analytical procedures frequently need to be improved to obtain reliable results. This paper reports such an improvement, which enables the chemical composition of various metal and inorganic materials to be determined with better sensitivity and precision.

Elemental analysis is routinely conducted at the Analytical Research Core for Advanced Materials (ARCAM) by using various instrumental analytical methods: inductively coupled plasma atomic emission spectrometry (ICP-AES), atomic absorption spectrometry (AAS), etc. A trace amount of alloyed elements in a metallic material is often assayed; for this purpose, procedures with higher sensitivity and precision need to be developed. This report describes two contributions to improving the analytical procedure that we published in 2015.

A simultaneous internal standard method of flame AAS was developed for determining the amount of alloyed nickel analyte in a steel sample [1]. An AAS instrument at ARCAM has a xenon short-arc lamp as the continuous radiation source and a high-resolution echelle monochromator. This instrument enabled us to measure the analyte and internal standard absorption simultaneously. In the present work, nickel (232.003 nm) and iron (232.036 nm) were selected to improve the precision of the analytical results. Test solutions containing 10 $\mu\text{g cm}^{-3}$ of nickel and 500 $\mu\text{g cm}^{-3}$ of iron were prepared. Repeated measurements ($n = 10$) were carried out. Nickel and iron absorbance values within 1.5–2.7% of the relative standard deviation (RSD) were obtained. On the other hand, the ratios of these absorbance values (Ni/Fe) were 0.7–1.4% of RSD. Therefore, the present Ni/Fe internal standard method can be applied for precise nickel quantification in steel. Certified reference materials were used for the validation of the present AAS method: JSS 171-7 containing 0.099 mass% of nickel and JSS 154-14 containing 0.505 mass% of nickel. By using accurate iron-matching calibration, the analytical results of the present internal standard method agreed with the certified values. In addition, greater precision was obtained: 0.6–1.0% of RSD.

The liquid–liquid extraction method suggested in our previous paper [2] was applied to ICP-AES for

determining trace nickel in a cobalt–chromium–molybdenum (CCM) alloy. With a multi-type ICP-AES, analysts might be faced with the problem of spectral interference of CCM matrix components against trace nickel (< 0.01 mass%). In the present work, liquid–liquid extraction was employed for solution preparation in order to measure nickel emission lines without spectral interference. Approximately 0.10 g of the CCM alloy was decomposed with hydrochloric and nitric acids or hydrofluoric acid. The resulting solution was fumed with 10 cm^3 of perchloric acid. By pipetting 35 mass% hydrochloric acid to the fumed solution, chromium was completely removed. Dried salt with no perchloric acid was dissolved in 20 cm^3 of diluted hydrochloric acid (containing a one-third volume of distilled water). Liquid-liquid extraction was carried out two times by using 20 cm^3 of 4-methyl-2-pentanone containing 20 vol% of trioctylamine. Perchloric acid (2 cm^3) was added to the resulting aqueous solution. Organic compounds in the aqueous solution were decomposed by adding nitric acid continuously. Finally, nickel in a 25.0 cm^3 solution with yttrium as an internal standard was measured by ICP-AES. The lower limit of determination was improved from 0.01 mass% (conventional ICP-AES procedure without liquid–liquid extraction) to 0.0006 mass% (the present method).

References

- [1] T. Itagaki, T. Ashino, K. Takada, and K. Wagatsuma, *Bunseki Kagaku* **64**, 117 (2015).
- [2] F. Sakamoto, T. Ashino, and K. Wagatsuma, *Bunseki Kagaku* **64**, 689 (2015).

Kenichi Nakayama (Corresponding Author, Analytical Research Core for Advanced Materials)

E-mail: ken1naka@imr.tohoku.ac.jp

Kazuaki Wagatsuma (Head of Analytical Research Core for Advanced Materials)

E-mail: wagatsuma@imr.tohoku.ac.jp

URL: <http://bunseki-core.imr.tohoku.ac.jp/>

Author Index

Name	page	Name	page
A			
Aoki, Dai	37	Mohri, Tetsuo	16, 45
Arima, Hiroshi	9	N	
Awaji, Satoshi	43	Nagai, Yasuyoshi	20, 40, 41
B			
Bauer, Gerrit Ernst-Wilhelm	47	Nagata, Shinji	21
Bedanta, Subhankar	47	Nagumo, Kazuaki	20
Belosludov, Rodion	46	Nakayama, Kenichi	52
C			
Chiba, Akihiko	13	Nambu, Yusuke	31
D			
Deb Nath, Sankar Kumar	45	Niinomi, Mitsuo	10
F			
Fujita, Masaki	48	Nojima, Tsutomu	50
Fujiwara, Kozo	18	Nojiri, Hiroyuki	27, 43
Furuhara, Tadashi	42	O	
G			
Goto, Takashi	12	Ogata, Shigenobu	45
H			
Hashimoto, Kenichiro	30	Orimo, Shin-ichi	24, 46
Hatano, Yuji	40	S	
Hirose, Yusuke	41	Saitoh, Eiji	28
I			
Imashuku, Susumu	14	Sasaki, Takahiko	50
Inoue, Koji	20	Satoh, Yuhki	22
Ishibashi, Shoji	16	Shimizu, Yasuo	20
Ito, Akihiko	12	Shiogai, Junichi	29
K			
Kato, Hidemi	23	Sugiyama, Kazumasa	9
Katsui, Hirokazu	12	T	
Kiguchi, Takanori	38	Takagi, Shigeyuki	24
Koyama, Chihiro	36	Takahashi, Ryo	28
Kubo, Momoji	19	Takanashi, Koki	35
M			
Makino, Akihiro	49	Takeuchi, Akira	49
Masahashi, Naoya	44	Tretiakov, Oleg	26
Matsuoka, Takashi	33	U	
Miyamoto, Goro	8	Uda, Satoshi	36
Miyasaka, Hitoshi	34	W	
X			
Xie, Guoqiang			
Y			
Yamamura, Tomoo			
Yonenaga, Ichiro			
Yoshikawa, Akira			
Yubuta, Kunio			

Keyword Index

Keyword	page	Keyword	page
A			
alloy	10, 13	magnetoresistance	35
anomalous X-ray scattering	9	mechanical properties	10, 12, 13, 15
atom probe tomography	8, 20	molecular dynamics	19
antiferromagnets	26	N	
B			
biological	10, 15	nanocluster	8
bulk metallic glass	15	nanostructure	12, 13, 38
C			
ceramic	12, 19	neutron scattering	31
crystal growth	11, 18, 33	nuclear materials	20, 22
crystal structure	24, 34	O	
cathodoluminescence	14	optical properties	30
D			
defects	32, 36	optoelectronic	33
deformation	32	organic	30
devices	11	oxide	36
dielectric properties	38	P	
doping	36	porosity	23
Dzyaloshinskii-Moriya interaction	26	positron annihilation	16
diffusion	20	R	
E			
electron irradiation	14, 22	radiation effects	11
electronic material	28	S	
energy storage	23	semiconducting	32
F			
Fermi surface	37	simulation	19, 22
ferromagnetic	34	solar cells	18
field-effect transistor	29	spectroscopy	14, 33
first-principles calculations	16, 24	spin current	28
foam	23	spin fluctuation	31
G			
glass	9	spintronics	28, 35
H			
half-metal	35	steel	8
heavy fermion	37	superconducting	27, 29, 30
high magnetic field	27	skyrmions	26
hydride	24	T	
hydrogen implantation	21	thin films	29
I			
ion beam analysis	21	transmission electron microscopy (TEM)	38
L			
luminescence	21	triangular antiferromagnet	31
M			
magnetic properties	34	V	
		vacancy	16
		X	
		XAFS	9
		X-ray scattering	27

Editors:

Atsushi Tsukazaki (IMR), Gerrit E.W. Bauer (IMR),
Kozo Fujiwara (IMR), Yusuke Nambu (IMR),
Junpei Okada (IMR), and Shigeyuki Takagi (IMR)

Editorial Staff:

Misa Yokoyama (IMR), Yoshiko Takahashi (IMR),
and Kaori Kikuchi (IMR)

Printing:

HOKUTO Corporation

Organization

Institute for Materials Research
Tohoku University
2-1-1 Katahira, Aoba-ku, Sendai 980-8577, Japan
Tel. +81-(0)22-215-2144 Fax. +81-(0)22-215-2482

URL: <http://www.imr.tohoku.ac.jp/>
E-mail: pro-adm@imr.tohoku.ac.jp



東北大学 金属材料研究所
Institute for Materials Research
Tohoku University

2-1-1 Katahira, Aoba-ku
Sendai 980-8577, Japan

<http://www.imr.tohoku.ac.jp/>